Global SM and BSM Fits using Results from LHC and other Experiments

Emanuele Bagnaschi[1], *Philip Bechtle*[2], *Johannes Haller*[3], *Roman Kogler*[3], *Thomas Peiffer*[4], *Tim Stefaniak*[1], *Georg Weiglein*[1]

[1]DESY, Hamburg, Germany
[2]Physikalisches Institut, Universität Bonn, Germany
[3]Institut für Experimentalphysik, Universität Hamburg, Germany
[4]II. Physikalisches Institut, Universität Göttingen, Germany

DOI: http://dx.doi.org/10.3204/PUBDB-2018-00782/B8

Global fits which confront results of High-Energy-Physics experiments with accurate theoretical predictions can be used to provide indirect constraints on fundamental parameters of the Standard Model of particle physics or new physics models. Important examples are global fits of the electroweak sector of the Standard Model or fits of supersymetric extensions of it. In this article we review the results obtained using the public software tools `Gfitter`, `Fittino`, `MasterCode`, `HiggsBounds` and `HiggsSignals` and we highlight the physics results of global fits in the Standard Model, Supersymmetry and various other beyond-the-Standard-Model theories.

1 Introduction

Models of fundamental physics are characterized by a set of free parameters, which cannot be calculated from fundamental model assumptions, but must be determined experimentally. Each of these parameters affects a large variety of observables because of the effects of radiative corrections. From a detailed comparison of accurate theoretical predictions with experimental observables and direct search results obtained at High-Energy-Physics (HEP) experiments, indirect constraints on the free parameters of particle physics models can be derived, and the overall consistency of these models with the data can be studied. Such comparisons enable insights into the model in mass regions even higher than the centre-of-mass energy available in the respective HEP experiments because of the effects of radiative corrections.

Often, these comparisons are performed with so-called global fits using software frameworks which provide tool-kits of sophisticated statistical methods for the interpretation of the fit results. These software tools provide implementations of accurate theoretical calculations or software interfaces to calculations implemented in external software. Furthermore, tools for model independent interpretations of measurements and search results can be integrated into the global fit frameworks, or applied by themselves to check the agreement of a certain physics model with the measurements.

In this article, a review is given of the results obtained using the software tools `Gfitter`, `Fittino`, `MasterCode`, `HiggsBounds` and `HiggsSignals` which have been developed in parts during the course of the SFB 676. We discuss the physics results in the Standard Model

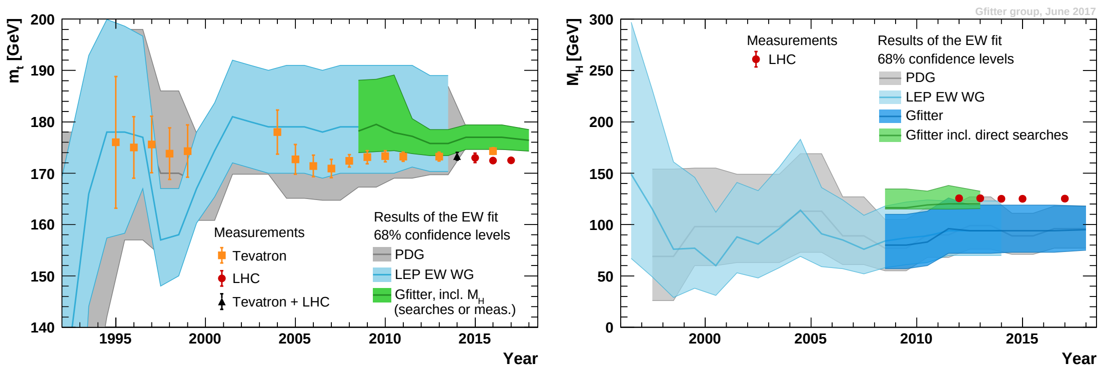

Figure 1: Prediction of the top quark mass (left) and the Higgs boson mass (right) within the Standard Model as a function of time as obtained by various analysis groups using electroweak precision data (grey [3], light blue [2], green [4]). Direct mass measurements after the top quark and Higgs boson discoveries are displayed by the data points. Figures taken from Ref. [11].

of particle physics (SM) and models of new physics with particular emphasis on supersymetric models and models with an extended Higgs sector. Furthermore, we highlight the developments during the last decade in this area, with a major impact arising from the discovery of a Higgs boson in 2012 at CERN's LHC.

2 Global fits of the electroweak sector of the SM

During the last decades, tremendous progress has been made in the experimental techniques to measure crucial observables of the SM as well as in theoretical calculations that have led to precise predictions of these observables within the SM. In particular, the precise measurements of electroweak data obtained during the 1990ies in e^+e^- collisions at the Z pole by the LEP collaborations and the SLD collaboration [1] have allowed the application of the techniques of global fits to obtain impressive results in the electroweak sector of the SM [2–5]. For an historical review of the results of global fits of the electroweak sector of the SM and a discussion of their perspectives the reader is referred to Ref. [6]. Results on the subject obtained within the SFB 676 using the `Gfitter` framework can be found in Ref. [7–13].

For a long time, these global fits have been used to derive indirect constraints on yet experimentally undetermined SM parameters. An impressive example of this kind is the correct indirect determination of the mass of the top quark m_t before its direct discovery at the Tevatron in 1995 [14, 15] as shown in Fig. 1 (left) where the indirect prediction of m_t as obtained in global fits by several groups is shown as a function of time as well as results from direct m_t measurements. Later, the discovery of the top quark and the measurement of its mass enabled the indirect determination of the mass of the Higgs boson M_H within the SM using global fits before the direct discovery of a Higgs boson at the LHC. The development of the M_H predictions obtained by several groups in global fits is shown in Fig. 1 (right) as a function of time. The combination of precise theoretical calculations, electroweak precision data, information on m_t and results from direct Higgs boson searches at LEP and the Tevatron have led to an indirect prediction of $M_H = 120^{+12}_{-5}$ GeV in 2011 [8] which was in impressive agreement with the direct discovery of a Higgs boson by the LHC collaborations in 2012 [16, 17] and their combined mass measurement of $M_H = 125.09 \pm 0.21 \pm 0.11$ GeV using the LHC run-1 data-set [18] .

With an interpretation of the discovered Higgs boson as the Higgs boson of the SM and with the measurement of its mass, the electroweak sector of the SM is complete and all fundamental SM parameters are directly measured. In this situation, global fits are a powerful tool for tests of the internal consistency of the SM, for the prediction of SM parameters with high precision, and for the derivation of constraints of theories describing physics beyond the SM (cf. Sect. 5). In the following we restrict ourselves to the discussion of the most recent results as obtained in this field of research within the SFB 676 by the `Gfitter` group [11] using latest experimental results and theoretical predictions. Earlier `Gfitter` results [7–10] are only mentioned to highlight recent changes and improvements.

The data used in the fits are the electroweak precision data at the Z pole and their correlations as measured by the LEP and SLD collaborations [1], the width [19] and the mass [11] of the W boson including information from measurements at LEP [20], Tevatron [21] and most recently from the ATLAS experiment [22], the world average values for the running quark masses [19], a measurement of the effective leptonic electroweak mixing angle by the Tevatron experiments [23], an up-to-date determination of the five-quark vacuum polarisation contribution to $\alpha(M_Z^2)$, $\Delta\alpha_{\rm had}^{(5)}(M_Z^2)$ [24], an average [11] of the top quark mass measurements as obtained by ATLAS and CMS in the run-1 data-set of the LHC and the combined ATLAS and CMS measurement of the Higgs boson mass [18]. The electroweak fit makes use of the most up-to-date theoretical calculations of the electroweak observables, mostly at NNLO accuracy. For a detailed list of calculations used in the fit, the reader is referred to [11].

Using these input data and theoretical calculations with the free fit parameters M_H, M_Z, m_c, m_b m_t, $\Delta\alpha_{\rm had}^{(5)}(M_Z^2)$ and α_S (plus ten additional theoretical uncertainty (*nuisance*) parameters), the global fit converges at a minimum χ^2 value of 18.6 for 15 degrees of freedom, which corresponds to a p-value of 0.23. In Fig. 2 (left), the difference between the global fit result as well as the input measurement with the indirect determination (obtained from a global fit excluding the experimental measurement of the observable in question) for each observable are shown in units of the total uncertainty (quadratic sum of uncertainties of indirect determination and input measurement). Analogue results for the indirect determinations, trivially centered around zero, are shown to illustrate the impact of their uncertainties on the total uncertainties. In general, a nice agreement is observed, with only few observables featuring deviations of more than 2σ. The strongest deviation is observed for the forward-backward asymmetry of b quarks, $A_{\rm FB}^{0,b}$, which is extensively discussed in the literature.

The experimental observables provide sensitivity to constrain the Higgs boson mass with different strength because of different impacts in the contribution of radiative corrections in their theoretical prediction. In Fig. 2 (right), the indirect determinations of M_H in the SM using the four observables providing the strongest M_H constraints are compared to the fit result including all data except the direct M_H measurement which results in $M_H = 90^{+21}_{-18}$ GeV and is in agreement with the direct M_H measurement within 1.7 standard deviations.

The indirect result for the mass of the W boson provided by the gobal fit is $M_W = 80.354 \pm 0.007_{\rm tot}$ GeV [11] which represents the most precise determination of M_W in the SM, even outperforming the direct measurement. The total uncertainty is not dominated by a single source but results from many different contributions of similar impact. The most important contributions are the theoretical uncertainty of M_W (contributing ± 0.0040 GeV to the

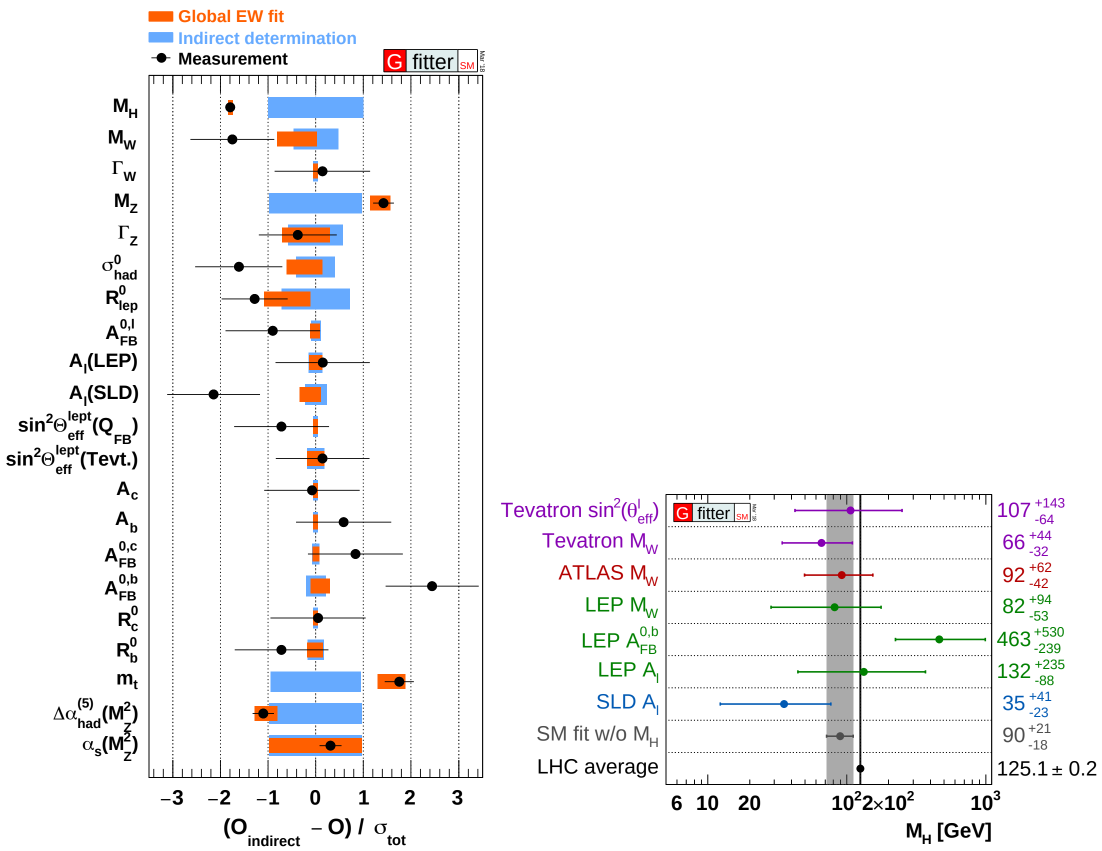

Figure 2: Results of the global electroweak fit: (left) comparison of the fit results and the input measurements with the indirect determinations in units of the total uncertainties for all observables used in the fit. (right) Comparison of the indirect prediction of M_H obtained from individual observables with the indirect global fit result and the LHC measurement of M_H. Figures taken from Ref. [11].

total uncertainty), the theoretical uncertainty on m_t (contributing $\pm 0.0030\,\mathrm{GeV}$), the experimental uncertainty on m_t (contributing $\pm 0.0027\,\mathrm{GeV}$), the uncertainty on M_Z (contributing $\pm 0.0026\,\mathrm{GeV}$), the uncertainty of α_S (contributing $\pm 0.0026\,\mathrm{GeV}$) and the uncertainty on $\Delta\alpha_{\mathrm{had}}$ (contributing $\pm 0.0024\,\mathrm{GeV}$).

Likewise, the indirect result of the global fit for the effective leptonic weak mixing angle is $\sin^2\theta^l_{\mathrm{eff}} = 0.23153 \pm 0.00006_{\mathrm{tot}}$ with dominating uncertainties resulting from the determination of $\Delta\alpha_{\mathrm{had}}$ (± 0.000035) and from the theoretical uncertainty on $\sin^2\theta^l_{\mathrm{eff}}$ (± 0.000040).

Other highlights of the physics results of the global fit are the indirect fit result for the mass of the top quark, $m_t = 176.4 \pm 2.1\,\mathrm{GeV}$, and the indirect fit result for the strong coupling strength at the scale of the Z boson mass, $\alpha_S(M_Z^2) = 0.1194 \pm 0.0029$, which is determined at full NNLO for electroweak and strong contributions and partially at NNNLO for strong corrections.

With a simultaneous two-dimensional indirect determination of m_t and M_W the internal

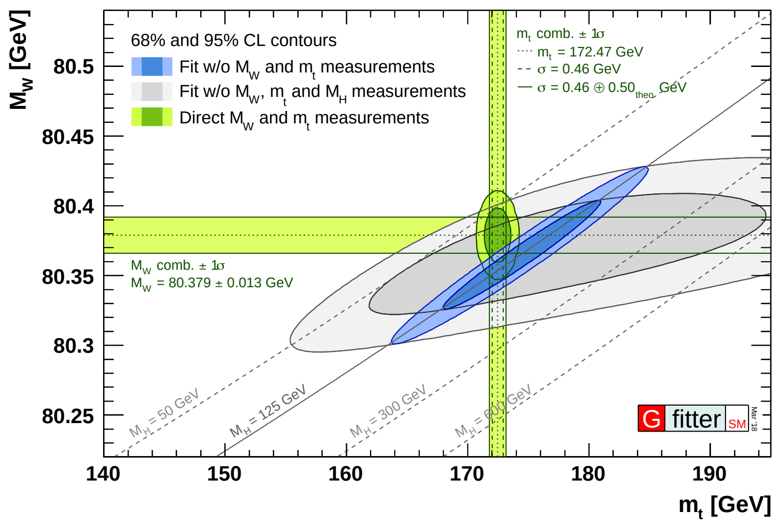

Figure 3: Internal consistency of the electroweak sector of the SM: allowed regions in the M_W versus m_t plane for the global fit including (blue) and excluding (grey) the LHC M_H measurement. The direct measurements of M_W and m_t are excluded from the fits. The fit results are compared to the direct measurements shown as green vertical and horizontal 1σ bands and two-dimensional 1σ and 2σ ellipses. Figure taken from Ref. [11].

consistency of the SM can be tested. In Fig. 3, the 68 % and 95 % confidence level (CL) allowed regions in the plane M_W versus m_t are shown for the global fit including all data except the direct m_t and M_W measurements (blue) and for a global fit excluding in addition the M_H measurement (grey). The strong impact of the precise M_H measurement is clearly visible by a huge reduction of the allowed parameter space. The fit results are compared to average values of the direct measurements of m_t and M_W shown in green error bands and ellipses. Good agreement between direct measurements and indirect determinations are observed.[1]

While the electroweak precision data measured in e^+e^- collisions at LEP and SLD still have a crucial importance for global fits of the electroweak sector, experimental results obtained during the last decades at hadron colliders have continuously improved the fit performance: notably, the precise measurements of the top quark mass and the W boson mass at the Tevatron and at the LHC, and, most importantly, the LHC determination of the mass of the Higgs boson. While future improved measurements of M_W and m_t can be expected at the LHC, the International Linear Collider (ILC) with GigaZ option will provide even better precision for these mass parameters, together with improved values for the partial decay width of the Z boson, R_l^0 and for $\sin^2\theta_{\rm eff}^f$ from measurements of the left-right asymmetry $A_{\rm LR}$. With these experimental improvements together with projected improvements in the theoretical calculations, a significant increase in the predictive power of the fit is found [10], where in particular the ILC/GigaZ scenario provides excellent sensitivity to indirect new physics.

[1] An additional theoretical uncertainty of 0.5 GeV is attributed to the average of the kinematic m_t measurements at the LHC due to the ambiguity in kinematic top quark mass definition, the colour structure of the fragmentation process and the perturbative relation between pole and $\overline{MS}$ mass.

3 Constraints from Higgs searches and measurements

Since the discovery of a Higgs boson [16, 17] one of the most important aims of HEP is to understand this particle in utmost detail, and to contrast its measured properties with the predictions of the SM and its possible new physics extensions. However, already before, the limits from collider searches both for a SM-like Higgs boson and for other more exotic scalar bosons posed important constraints on Higgs boson properties which had a large impact on the construction of alternatives and extensions of the SM. The same is true after the discovery of a SM-like Higgs boson for searches for additional scalar bosons. The constraints on their properties obtained from search limits continue to play an important role in model building and phenomenology.

In this section, we introduce two tools developed in parts in the context of the SFB 676. The code `HiggsBounds` deals with model independent exclusion limits on SM-like Higgs bosons and other scalar bosons. It incorporates the legacy of exclusion limits from searches at the LEP and Tevatron experiments. `HiggsSignals`, on the other hand, incorporates the experimental measurements of the discovered Higgs boson's properties, including its mass, production and decay rates, and kinematical information in the form of Simplified Template Cross Section (STXS) results.

3.1 HiggsBounds

Before the LHC, the most stringent limits on a SM-like Higgs boson were set by the LEP experiments [25]. Also the Tevatron searches showed sensitivity for a SM Higgs boson interpretation, especially around a Higgs boson mass of $m_{\mathrm{h}} \approx 2m_{\mathrm{W}} \approx 160\,\mathrm{GeV}$ [26]. In addition, a variety of searches for non-standard Higgs bosons were carried out at LEP [27] and the Tevatron, where the latter ones resulted in important constraints on 2HDM or SUSY interpretations for large $\tan\beta$ (see e.g. [28, 29]). The experimental searches, previously at LEP and the Tevatron and nowadays at the LHC, are carried out in many different channels. For instance, already at LEP the search for a neutral Higgs boson was performed in Higgsstrahlung, in WW and ZZ fusion, in the Yukawa process, and in pair production. The final states of the searches at LEP, the Tevatron and the LHC incorporate SM Higgs decays such as $h \to \gamma\gamma, ZZ, WW, gg, b\bar{b}, \tau\tau, \mu\mu$, as well decay modes that are motivated by new physics scenarios, e.g. into invisible particles. In addition, new physics models like the 2HDM and MSSM feature a charged Higgs boson giving rise to further decay signatures. In total, a plethora of different search results has been obtained, most of which have been presented both in specific model interpretations and as model-independent limits on the signal cross section for a specific Higgs mass and a specific combination of the production and decay modes. Making use of this wealth of experimental information to constrain the parameter space of different models is a non-trivial task.

With `HiggsBounds` [30–32] a common tool is provided which deals with the problems of finding the most significant limit and of deciding whether a particular search limit is valid for any given new physics model containing an arbitrary number of neutral and charged scalar bosons. The theoretical input of `HiggsBounds` is provided in terms of physical quantities predicted by the new physics model, i.e. the number of charged and neutral Higgs bosons, their masses, total decay widths, production and decay rates. The production rates can either be approximated in the code from effective couplings, or directly specified at the partonic or hadronic level. Similarly, the decay rates are estimated from effective couplings or given directly by the user. In this way, `HiggsBounds` is independent of the internal details of the new physics model, and applicable to basically any model.

A first challenge occurs in tests of a model against several observed limits at a specific CL in parallel. For instance, for limits given at 95% CL the chance to wrongfully exclude a signal model is $\leq 5\%$ for each tested limit, and after n tests the true CL of the model exclusion might be as low as $1 - 0.95^n$. While such a dilution of the CL is not intended, it was often ignored in phenomenological studies. However, a proper statistical combination of various limits usually requires more information (e.g. correlations between systematic uncertainties) than is typically publicly available. The procedure implemented in `HiggsBounds` is a test of the model only against the limit of the most sensitive search which represents a well-defined, conservative and CL preserving statistical procedure. The sensitivity of a search can be determined by comparing the model predictions with the expected exclusion limit.

A second challenge arises from the validity of a given limit in a certain model. A typical example are the assumptions made in the derivation of published limits on the composition of Higgs production and decay modes, like in combined searches for a SM Higgs boson at LEP, Tevatron or the LHC, where it is assumes that all combined search channels contribute to the signal in the same fraction as predicted by the SM. In order to test whether such a limit is valid in a certain model, `HiggsBounds` checks whether the model-predicted signal fractions of the relevant channels, weighted with their absolute size, are within a very small (user configurable) band around the assumption used for the limit generation [33].

In addition to the exclusion test with respect to a fixed 95 % CL, an improved implementation of exclusions is possible if the full likelihood of the exclusion fit is available. Since `HiggsBounds` version 4.1 [33] an approximate likelihood function for the LEP exclusions is provided. After the Higgs discovery, these exclusions are still highly relevant for new physics models that contain an additional lighter Higgs boson. Assuming Gaussian behaviour, the likelihood approximation is provided as a χ^2 contribution for every mass point and for every signal strength parameter $\mu = [0.001, 1]$ for which the CL_{s+b} value has been retained in the LEP model independent limits. Such an (approximate) likelihood for exclusions from Higgs searches is useful in global fits, and it would be desirable to have more such likelihoods available, in particular for the recent LHC results.

The first publication of model-independent likelihoods instead of 95% CL limits at the LHC was performed by the CMS experiment in the search for non-standard (heavy) Higgs bosons in the $\tau^+\tau^-$ final state [35], using a single scalar narrow resonance (ϕ) toy model. In Ref. [34] a description is given of the `HiggsBounds` procedure for the reconstruction of the exclusion likelihood from this data for arbitrary Higgs models and its application on MSSM benchmark models. The likelihood information allows a statistically consistent combination of the information on limits from searches for additional Higgs bosons with the measurements of the observed SM-like Higgs boson. The tools `HiggsBounds` and `HiggsSignals` (see below) provide a framework for this task and can be applied to arbitrary models with scalars. Figure 4 exemplifies the use of the likelihood information from the CMS $pp \to \phi \to \tau^+\tau^-$ search. In Fig. 4 (left) one example of the likelihood values is shown for fixed Higgs mass $m_\phi = 300\,\mathrm{GeV}$ as a function of the cross sections of the two main production modes, gluon fusion ($gg \to \phi$) and b-associated Higgs production ($b\bar{b} \to \phi$). Many models of new physics change the ratio of these cross sections. This three-dimensional grid of likelihood values is then interpolated in `HiggsBounds` and allows one to reproduce the model dependent limit in the $m_h^{\max}$ benchmark scenario to very high accuracy, as shown in Fig. 4 (right).

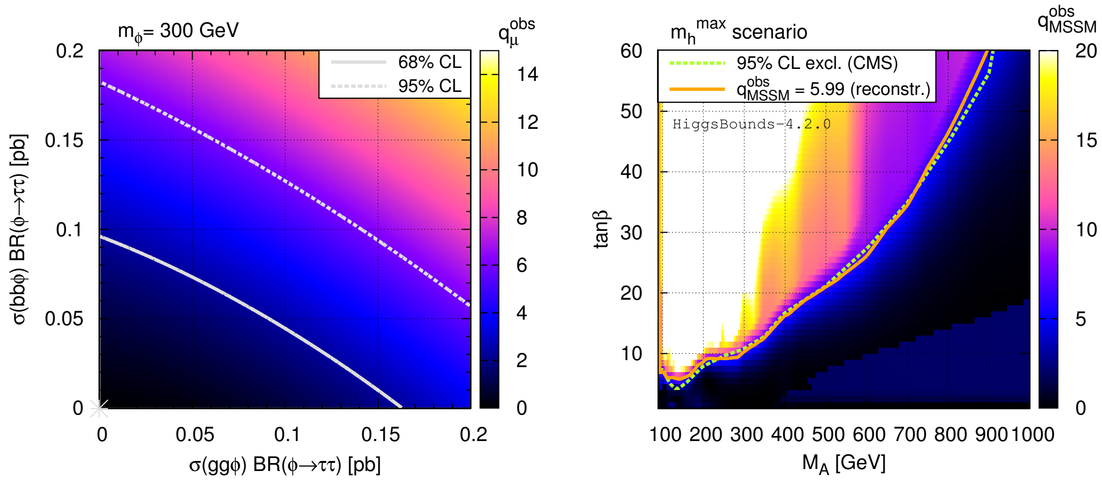

Figure 4: Input and validation of the exclusion likelihood reconstructed by `HiggsBounds` [34] for the CMS search for $pp \to \phi \to \tau^+\tau^-$ [35]. The likelihood input (left) is provided for a single scalar narrow resonance (ϕ) toy model for varying masses m_ϕ and cross sections in the dominant production modes $gg \to \phi$ and $bb \to \phi$. The implementation is validated by comparing the likelihood-based exclusion (right) in the $m_h^{\max}$ benchmark scenario with the official CMS limit, yielding excellent agreement. Figures taken from Ref. [34].

3.2 HiggsSignals

Since any new physics extension of the SM has to feature a particle with properties consistent with the measured properties of the Higgs boson, an important task is a comparison of the model predictions with the Higgs boson measurements at the LHC. While a large amount of sensitive model interpretations have been published by ATLAS and CMS (see e.g. Ref. [36] for the LHC run-1 results), not every new physics model can be tested against these results as these are based on specific model assumptions. The aim of `HiggsSignals` [32, 37–39] is the usage of model-independent experimental results — the mass measurements and the signal strength measurements (or, equivalently, absolute signal rate measurements) — in each individual search channel and kinematical configuration studied by the experiments. `HiggsSignals` calculates a χ^2 value that quantifies the level of (dis-)agreement between model predictions and measurements by decomposing the given uncertainties on the rate measurements into all theoretical sources of systematic errors, all known correlated experimental systematic errors, and a remainder that contains the statistical uncertainty and remaining publicly inseparable experimental systematic uncertainties. This decomposition enables the code to take into account the major correlations among the measurements. Furthermore, `HiggsSignals` incorporates all available information on the sub-channel composition of each rate measurement, which depends on the relative efficiency of the different Higgs production and possibly decay modes in the experimentally analysed search channel. If public information on these efficiencies is available, it is included by default.

The current public version [32] offers in addition the implementation of Simplified Template Cross Section (STXS) [40] results which contain experimental results binned in kinematical configurations which promise sensitivity on the vertex structure of the Higgs boson production

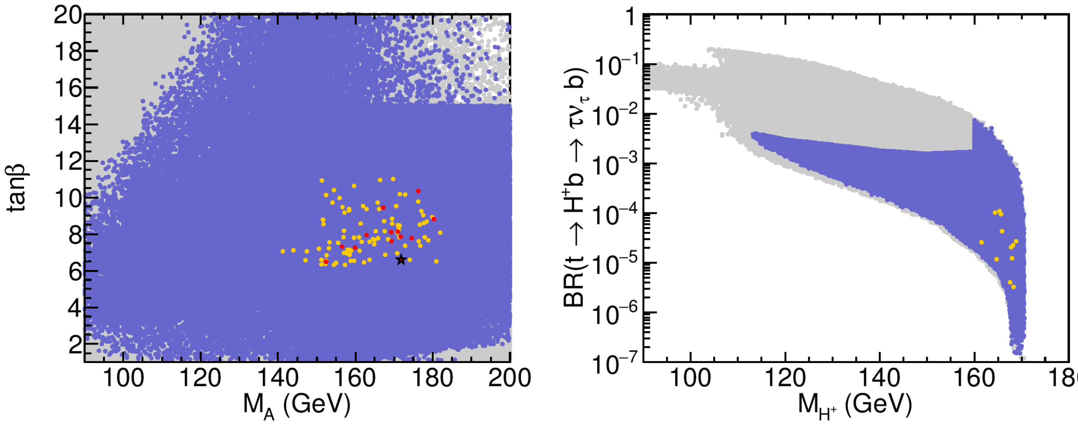

Figure 5: Result from a scan of the phenomenological MSSM with eight parameters using `HiggsBounds` and `HiggsSignals` for the case where the heavier CP even Higgs boson H is identified with the observed Higgs boson at $m_{\rm H} = 125\,{\rm GeV}$ [41]. The red and yellow points correspond to the 1 and 2σ-level, respectively, while allowed points outside the 2σ region are indicated in blue. The left plot shows the allowed points in the (M_A, $\tan\beta$) parameter plane, while the right plot shows the combined branching fraction for the top quark decaying to a charged Higgs boson $H^\pm$ and a b-quark, and $H^\pm$ decaying to $\tau\nu_\tau$. Figures taken from Ref. [41].

through e.g. the transverse momentum spectrum of the Higgs boson or additional objects in the event.

The power of combining `HiggsBounds` and `HiggsSignals` is e.g. illustrated in the study of the parameter space of the eight-dimensional phenomenological MSSM [41], where different possible interpretations have been identified: Either the light Higgs boson h can be identified with the observed particle at 125 GeV, and the other Higgs particles are heavy ("decoupling limit"), or one of the neutral CP even Higgs bosons becomes SM-like despite the further Higgs spectrum being light ("alignment without decoupling"). The latter happens within the MSSM only in a rather specific parameter region, and provides the possibilities that either the lighter or the heavier CP even Higgs boson can be identified with the SM-like state at 125 GeV. Interestingly, the heavier Higgs boson (H) interpretation of the signal is still allowed after taking into account all LHC run-1 Higgs measurements and limits from ATLAS and CMS, as well as constraints from flavour physics. Some scan results for this interpretation are shown in Fig. 5. Fig. 5 (left) illustrates in the (M_A, $\tan\beta$) parameter plane that the allowed points (in yellow and red) are clustered in a very restricted parameter space, as they are constrained from many complementary searches. The branching fraction for top quarks decaying into a light charged Higgs boson $H^\pm$ with successive decay to $\tau\nu_\tau$ is shown in Fig. 5 (right), indicating that the remaining viable parameter points are located at the kinematic threshold (or beyond) of this decay such that they escape the exclusion limit. It should be noted that the situation where the SM-like Higgs boson at 125 GeV is not the lightest state in the Higgs spectrum occurs generically in extensions of the SM with an additional Higgs singlet as it is the case in the NMSSM, see e.g. Refs. [42, 43].

The exploration of the mechanism of electroweak symmetry breaking via precision investigations in the Higgs sector will continue to be one of the prime topics of elementary particle physics during the next decades. The prospective improvements in the experimental precision in combination with corresponding efforts on the theory side will significantly enhance the sensitivity for discovering small deviations from the SM. Tools like `HiggsBounds` and `HiggsSignals` will continue to play an important role in this research field, enabling quick and rather precise tests of new physics models with any number of scalars against the experimental results thus allowing to easily identify the phenomenologically relevant parameter space of the model.

4 Global fits of supersymmetric models

For tests of the compatibility of the experimental data with scenarios of physics beyond the SM, it is of high interest to study well-motivated complete and renormalizable extensions of the SM, like Supersymmetry, which provide a more fundamental theory beyond the SM with a broader range of explained features of nature. The ability to calculate loop corrections to a wide variety of precision measurements, like the properties of electroweak symmetry breaking and the Higgs boson, and the ability to calculate cosmological predictions, increases the predictive power and accordingly the falsifiability of such a theory dramatically.

Besides many strong theoretical arguments for supersymmetric extensions of the SM, at least two observations which indicate deviations from the SM prediction could be a first experimental hint towards the realisation of SUSY in nature: First, the observed dark matter (DM) content in the universe [44], which is naturally explained by a neutral particle with a weak coupling and a mass near the electroweak scale, and second, the measurement of the anomalous magnetic moment of the muon $(g-2)_\mu$ which deviates from the SM prediction [45]. On the other hand, no SUSY particles have been found so far. Thus, it is interesting to contrast these experimental constraints and the electroweak precision measurements, including the measurement of the Higgs boson mass, with the limits from direct searches for SUSY particles by means of global fits. In the next sections we introduce the global fitting tools `Fittino` and `MasterCode` which have partially been developed and extensively used within this project.

Since SUSY can be implemented in a wide variety of theoretical models with a large number of free parameters, it is desirable to start its investigation in global fits with models which are constrained by additional theoretical assumptions and symmetries leading to a more restricted number of free parameters. One of the models studied extensively in the following, is the constrained Minimal Supersymmetric Standard Model (cMSSM or CMSSM), which is defined by only four parameters, three of which are specified at the grand unification scale, and a sign. Other models studied are the so-called Phenomenological MSSM with 10 (pMSSM10) [46] and 11 (pMSSM11) [47] parameters, the NUHM1(2) in which universality is relaxed for both together (each separately) of the soft SUSY-breaking contributions to the masses-squared of the Higgs multiplets (see references in [48,49]), a SU(5)-GUT inspired scenario [50] and a scenario with Anomaly Mediated Supersymmetry Breaking (mAMSB) (see references in [51]).

4.1 Fittino

`Fittino` [52] is a global fitting tool for models beyond the SM (in particular SUSY) aiming at the LHC era and the yet-to-begin era of precision measurements of new physics at a high-energy e^+e^- collider. A list of citations to other global fit tools in this area is given in [53]. A global SUSY fit is sensitive to observables from SM precision measurements, cosmological measurements like the DM relic density, results from astroparticle physics (like direct and indirect DM annihilation and detection results), Higgs boson limits and properties, results from flavour physics, and exclusion limits from direct SUSY particle searches. In a series of publications [54–57] the impact of these experimental results on SUSY models was explored and projections for future colliders [58] have been obtained.

The results showed two consistent constraints pushing the cMSSM into the region of high sparticle mass scales: The relatively high Higgs boson mass requires large third generation squark masses to generate large enough loop effects on the Higgs mass, to lift it from its maximally allowed tree level value of m_Z up to around 125 GeV. At the same time, the direct LHC searches push the first generation squark masses above 1 TeV.

In the attempt to exclude the cMSSM [53] the `Fittino` collaboration faced a number of conceptual and technical challenges. First, SUSY exclusions are typically derived by defining a CL of e.g. $\mathrm{CL} < 0.05$ as a criterion for exclusion, where the CL is derived from a hypothesis test consisting of a likelihood ratio between two competing hypotheses: the null hypothesis, often the SM, and the alternative hypothesis, often SUSY. This approach works for a comparison of isolated features of a model, such as the search for a set of sparticles, or the search for an extended Higgs boson sector. However, for an attempt of a global exclusion of a SUSY model the null hypothesis would trivially fail the test since the DM relic density simply can't be explained in the SM. Of course, SUSY could be tested against the SM with an ad-hoc-assumption of some unexplained solution for DM. But since SUSY decouples, the cMSSM trivially becomes a SM with DM, if the SUSY mass scale is driven to infinity, and the two models in the hypothesis test would be asymptotically identical. For this reason, the remaining solution is to give up on the sensitivity of the Neyman-Pearson approach of likelihood-ratio based hypothesis tests, and just trivially test the goodness-of-fit of the cMSSM global fit to the data.

For most SUSY fits cited above, a Markov Chain Monte Carlo (MCMC) based approach, or other stochastic alternatives, for efficient scans of the parameter space are used. For an overview and comparison of approaches, see [59]. For a model with four continuous SUSY parameters and a few SM parameters, such as the cMSSM, about one billion scanning points with a valid SUSY sparticle spectrum are required to make a meaningful statement about the uncertainties, which represents a significant obstacle for the determination of the goodness of fit using a toy-Monte-Carlo based approach, since the computer codes for the calculation of the observables (see e.g. [60–63]) easily use about 20 seconds per SUSY parameter points. A toy-Monte-Carlo based approach is however indispensable for determining the goodness-of-fit, as a very large number of scan points is needed because of the behaviour of the model: The dependence of the observables on the parameters is highly irregular. The fit spans regions from low-scale SUSY with gauginos and sleptons in the $\mathcal{O}(100\,\mathrm{GeV})$ range, where the LHC exclusion can change rapidly within a few GeV, up to the decoupling regime where the prediction becomes independent of the parameter value. In addition, the prediction of the DM density depends critically on the interplay between different SUSY particles, and the fit covers different co-annihilation and focus-point regions [53], all with different relations between parameters and observables. Finally, the fit behaviour can change rapidly between regions with a physical spectrum and a forbidden tachyonic spectrum, or between the neutral lightest SUSY particle and the charged lightest SUSY particle.

In [53] a high-statistics toy fit of the cMSSM was performed for the first time. The goodness-of-fit test in Fig. 6 (right) sees the cMSSM just excluded at $\mathrm{CL} < 0.05$. In the figure, the smooth line shows the χ^2 distribution expected for fully gaussian uncertainties and fully linear relations between all observables and all parameters. However, the histogram illustrates the influence of non-gaussian errors, non-linearities and the effect of one-sided limits which distort the real

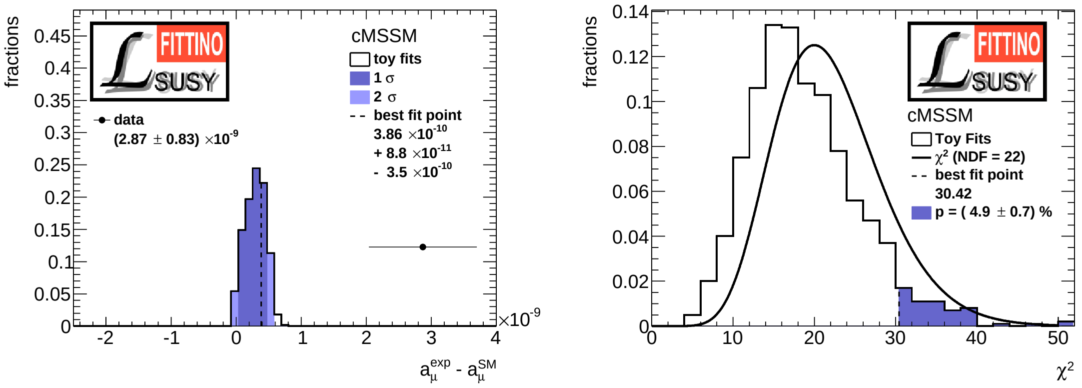

Figure 6: Results from the cMSSM exclusion: the tension between the prediction of $(g-2)_\mu$ and the experimental result (left) and the result of the toy-experiment based χ^2 distribution, which emanates from the inability of the fit to both accommodate $(g-2)_\mu$ and the negative LHC search results (right). Figures taken from Ref. [53].

toy-Monte-Carlo based distribution.

The observed CL critically depends on the choice of observables, much more so than when discussing parameter estimations. In the latter case, if one parameter affects several separate observables in a correlated way, it makes no difference whether all separate observables are fitted directly, or whether the separate observables are first combined and then a fit to the combined experimental result is performed. However, in the former case, the splitting of the sensitivity over many observables for which the theory prediction is largely correlated dilutes the goodness-of-fit test, since meaningful deviations between best fit and observations drown with respect to many random variations. In reality, it is not straightforward to optimize the observable selection while avoiding a bias on the result. The possible inputs to the global fit are discussed in [53], and some extreme choices do not allow an exclusion of the cMSSM with CL < 0.05. However, it is not possible to shed new light on this question before the muon anomalous moment $(g-2)_\mu$ is measured with better precision, and before its theory uncertainty does not decrease, as illustrated in Fig. 6 (left), where the uncertainty range of the toy-Monte-Carlo based fits is shown in the coloured distribution, and the measurement of $(g-2)_\mu$ is shown in the data point with experimental and theoretical uncertainty. The fit results fulfill the constraints of the LHC sparticle mass exclusions and the SM-like Higgs-boson properties, and thus no room is left to explain one of its two main motivations. Effectively, the cMSSM has become a SM with DM, forced to do so by the LHC results.

Ongoing work focuses on making global fits with a very large number of scanned SUSY parameter points in models beyond the cMSSM as flexible as possible. While a number of fits of the pMSSM exists (see e.g. Section 4.2), each model typically either requires its own implementation of parametrisations of LHC limits, or is limited to a small number of scan points, many orders of magnitude lower than the order of 1 billion required for realistic uncertainty estimates. One possible solution to this problem is presented in the code `SCYNet` [64]. Under the assumption that the dependence of the exclusion likelihood (cf. Fig. 4 (left)) on the relevant parameters is typically much more smooth and regular than the dependence of the global fit likelihood ratio or χ^2 on the parameters, the LHC sparticle exclusion likelihood can

Nuisance parameters	Electroweak precision observables
M_Z, M_T, $\Delta\alpha_{\rm had}$	M_W, A_b, A_c, $A^{0,b}_{FB}$,$A^{0,c}_{FB}$, $A^{0,l}_{FB}$, $A_l(P_\tau)$, $A_l(SLD)$, Γ_Z, R^0_b, R^0_c, R^0_l, $\sigma^0_{\rm had}$, $\sin^2\theta^l_{\rm eff}(Q^{\rm had}_{FB})$, a_μ
Higgs physics	**Flavour Constraints**
h_{125} properties $A/H \to \tau^\pm\tau^\mp$ searches	${\rm BR}_{B\to X_s ll}$, ${\rm BR}_{K\to l\nu}$, ${\rm BR}_{K\to\pi\nu\bar\nu}$, ${\rm BR}_{B\to X_s\gamma}$ ΔM_{B_s}, $\frac{\Delta M_{B_s}}{\Delta M_{B_d}}$, ${\rm BR}_{B_{s,d}\to\mu^\pm\mu^\mp}$, ϵ_k
Collider	**Dark Matter**
LEP, LHC run-1, LHC run-2	$\Omega_{CDM}h^2$, $\sigma^{\rm SI}_p$, $\sigma^{\rm SD}_p$

Table 1: Overview of the constraints included in a typical MasterCode analysis.

be parametrised independently of the rest of the global fit, using a much smaller number of scanning points. In SCYNet, this is explored using a deep Neural Net to perform a regression on the likelihood ratio output of a significant number of SUSY searches at ATLAS and CMS, implemented in a fast detector simulation and event selection using the tool CheckMATE [65]. Presently, a precision of the neural-net based regression compared to the simulation of the order of $-2\Delta\ln\mathcal{L} \approx \chi^2 \approx 1$ is achieved. At least the 2σ allowed range is described sufficiently precisely.

Based on such and other competing approaches, more complex models can be studied in the future. Currently, no direct positive experimental hint for SUSY beyond the tried-and-tested cosmological DM and $(g-2)_\mu$ has arisen. However, flavour physics holds the promise of anomalies (see e.g. [66] for an overview), which yet are waiting for a consistent interpretation in a UV-complete model.

4.2 MasterCode

MasterCode is a frequentist global-fitting framework which interfaces several different codes that provide state-of-the-art predictions for a wide range of observables of phenomenological interest using SLHALib [67,68]. Among these codes, we mention: the spectrum generator SoftSUSY [69]; FeynHiggs [63, 70–73], HiggsBounds [30, 31, 33, 34] and HiggsSignals [38, 39] (see above) for the Higgs sector observables and search limits; micrOMEGAs [74] and SSARD[2] for DM observables; SuFla [75,76] and SuperISO [61,77,78] for the flavour sector; FeynWZ [79–81] for the Electroweak Precision Observables (EWPOs). The sampling of the multidimensional parameter space of the model under analysis is performed using the MultiNest algorithm [82–84]. For an easy deployment of the framework on batch clusters a container-based approach with the udocker middleware [85] is used. An overview of constraints used in a typical MasterCode analysis is given in Tab. 1.

[2] SSARD is a private code developed by K. Olive and collaborators.

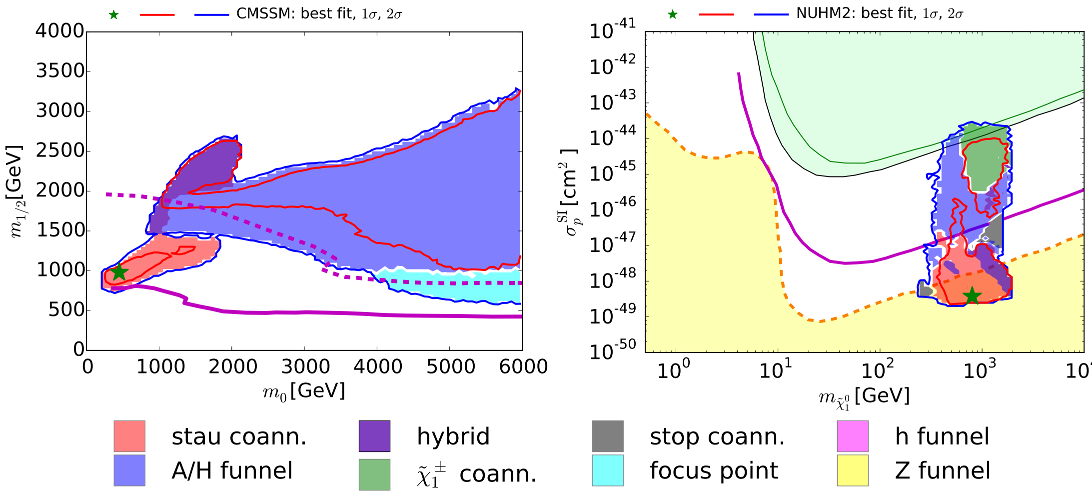

Figure 7: The relevant mechanisms to obtain the observed DM relic density (colour shadings), at 95%CL, in the m_0-$m_{1/2}$ plane of the CMSSM (left) and in the $m_{\tilde{\chi}_1^0}$-σ_p^{SI} of NUHM2 (right). In the left plot, the solid purple contour represents the LHC run-1 95% CL exclusion from $E_{T,\rm miss}$ searches, while the dashed purple contour shows the prospective 5σ discovery reach for $E_{T,\rm miss}$ searches at the LHC with 3000/fb at 14 TeV, corresponding approximately to the 95% CL exclusion sensitivity with 300/fb at 14 TeV. In the right plot, the black and green lines show the sensitivity of XENON100 and LUX back in 2015, while the purple one is the projected 95% exclusion sensitivity for LZ. Figures taken from Ref. [86].

4.2.1 Scenarios with specific SUSY-breaking patterns

While GUT-inspired scenarios and minimal Anomaly-Mediated Supersymmetry Breaking (mAMSB) provide theoretically inspired and elegant approaches towards possible UV completions, these models are all unable to explain the observed deviation from the SM prediction in the $(g-2)_\mu$ measurement. Nevertheless we consider the study of these scenarios an interesting and worthwhile effort, since the scientific community is still in the process of verifying the significance of this anomaly, both from the theory and experimental sides.

In [86] we have reappraised our CMSSM, NUHM1 and NUHM2 studies, with the aim of studying in more detail the DM phenomenology of these scenarios. Specifically, we were interested in the mechanisms which allow a recovery of the observed DM relic density. We started from the samples obtained in the study presented in refs. [48, 49] and then, in a given mass-plane, for each point selected after likelihood profiling we inferred the relevant process from the spectrum configuration. In other words, we defined a set of phenomenological "dark matter measures" to classify the points. For instance, points for which the relation $\left(m_{\tilde{\tau}_1}/m_{\tilde{\chi}_1^0}\right) < 0.15$ is satisfied were assigned to the process "stau co-annihilation". We cross-checked our approach with the explicit computation from `micrOMEGAs`, verifying that these DM measures are accurate in the vast majority of the cases. Two example results obtained in this analysis are illustrated in Fig. 7 where the m_0-$m_{1/2}$ plane in the CMSSM (left) and the $m_{\tilde{\chi}_1^0}$-σ_p^{SI} plane in the NUHM2 scenario (right) is shown. From this kind of results, one may appreciate how different mechanisms characterize the different allowed regions of the two models. Moreover, the study points

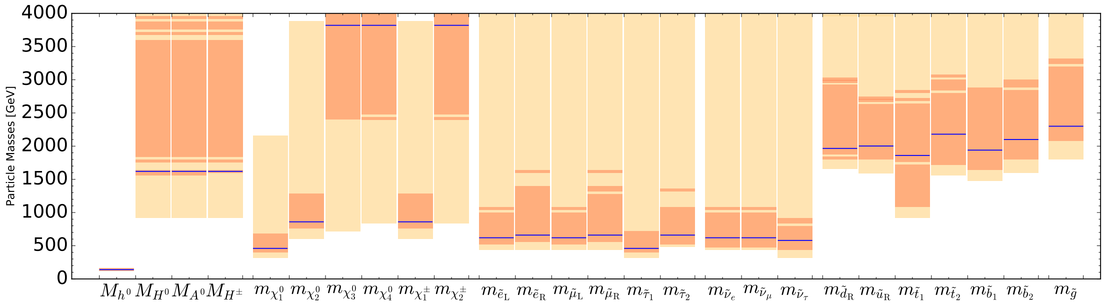

Figure 8: The allowed mass ranges at 68% CL (dark peach) and 95% CL (bright peach) in the SU(5)-GUT inspired scenario. The mass values corresponding to the best fit point are shown as horizontal blue lines. Figure taken from Ref. [87].

out the complementarity of information obtained from collider and direct detection experiments in these two scenarios.

We extended our studies with an analysis of an SU(5)-GUT inspired scenario [87] and an analysis of mAMSB [51]. In these papers the relevant constraints on superpartners production coming from LHC runs at 13 TeV have been implemented for the first time. For the sampling of the parameter space, the likelihood has been modelled following the `FastLim` [88] approach. In this approach, the relevant topologies for a given model have been identified and for each one of them the upper-limit on the cross-section at 95% CL provided by the experiments has been compared with the actual cross-section of the point being sampled, using a simple rescaling law to model the likelihood. In this way, a full MC simulation is avoided, since the elements needed (ie. the cross-section and the relevant branching ratio) can be computed using dedicated computer codes, such as `NLL-fast` [89,90], with very high performances. Higgs searches are implemented with a similar approach, using the cross-section times branching-ratio values computed by `FeynHiggs`.

The SU(5)-GUT study has revealed that, in contrast to the CMSSM/NUHM1/NUHM2 scenarios, also the co-annihilation mechanisms with either a $\tilde{\nu}_\tau$ or with $\tilde{u}_R$ or $\tilde{c}_R$ play a role because of the different pattern of the boundary conditions for the soft SUSY-breaking masses. In Fig. 8 the allowed mass range for the BSM particles in the SU(5)-GUT scenarios, at 68% CL (dark peach) and at 95% CL (bright peach) is shown as a typical outcome of a global `MasterCode` analysis. The mass values of the best fit point are indicated as horizontal blue lines. The figure illustrates the impact of the LHC results in providing stronger lower bounds for the coloured superpartners and for the other Higgs states of the MSSM. On the other hand, the allowed mass range of purely electroweakly interacting sparticles is less dependent on LHC search results.

The mAMSB study showed that a Wino-like or an Higgsino-like neutralino can fulfil the role of a DM candidate, with an upper bound on the neutralino mass of $m_{\tilde{\chi}_1^0} \lesssim 3$ TeV to avoid violating the bound coming from the observed DM relic density. Fig. 9 shows the two-dimensional likelihood profiles in the m_0-$m_{3/2}$ plane (left) and in the $m_{\tilde{\chi}_1^0}$-$m_{\tilde{\chi}_1^0}$ plane (right). In both cases, the colour shading reflects the nature of the neutralino. The left plot shows that the LSP is Wino-like only for a restricted range of $m_{3/2}$ values, while the Higgsino case is allowed for a larger range. The right plot displays the strict correlation between the neutralino nature and its mass, required by the relic density constraint.

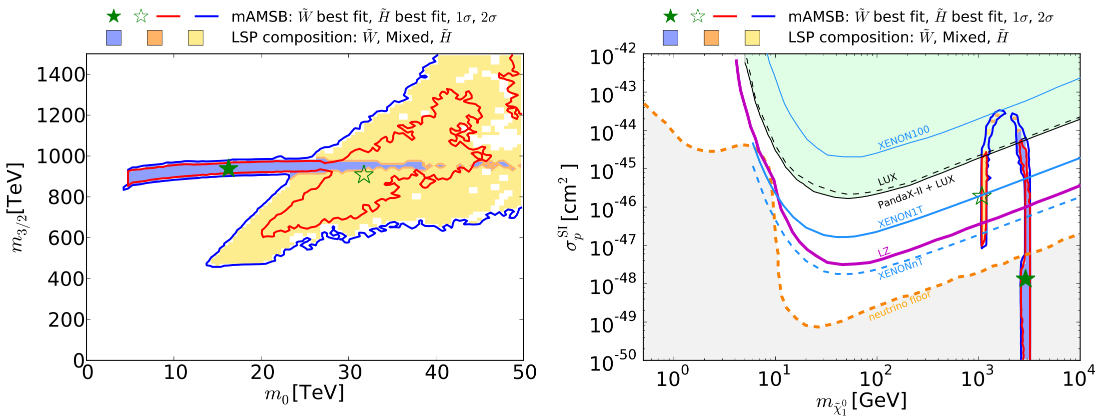

Figure 9: On the left (right), we show the two-dimensional likelihood profiles at 68% CL and at 95% CL in the m_0-$m_{3/2}$ ($m_{\tilde{\chi}_1^0}$-$\sigma_p^{\rm SI}$) plane in mAMSB. The colour shadings reflect the nature of the LSP, which can be either Wino-like (blue), Higgsino-like (yellow) or an admixture of the two (orange). Figures taken from Ref. [51].

In addition, a study of the CMSSM was performed in the so called "sub-GUT" flavour [91] in which the input scale of the soft SUSY-breaking terms, $M_{\rm in}$, is one of the parameters over which the sampling is performed and it is not fixed to be the GUT-scale. The one-dimensional likelihood profile for $\log(M_{\rm in})$ shown in Fig. 10 (left) features a slight preference, at the level of $\Delta\chi^2 \simeq 3$ for $M_{\rm in} \simeq 10^5$ GeV and for $M_{\rm in} \simeq 10^9$ GeV with respect to the case $M_{\rm in} \simeq M_{GUT}$ (i.e. the usual CMSSM scenario). The reason for this preference for lower $M_{\rm in}$ is a better compatibility with the latest $\mathrm{BR}(B_{s,d} \to \mu^\pm\mu^\mp)$ measurements. The two-dimensional likelihood profiles in the $\log(M_{\rm in})$-m_0 plane show the non-trivial dependence of m_0 on the scale $M_{\rm in}$.

4.2.2 Phenomenological scenarios

Besides studies of MSSM scenarios with definite SUSY-breaking patterns, phenomenological scenarios have been studied which are able to explain the observed $(g-2)_\mu$ anomaly. Moreover, allowing for lighter SUSY-spectra, they can be used to assess the possibility of a MSSM discovery at future LHC runs or at a future e^+e^- collider. We have focused our attention to the pMSSM10 and pMSSM11.

The pMSSM10 is indeed able to fit $(g-2)_\mu$, differently from various GUT scenarios, as can be seen from a comparison of the likelihoods displayed in Fig. 11 (left). Fig. 11 (right) display the two-dimensional likelihood profiles in the $m_{\tilde{\chi}_1^0}$-σ_p^{SI} plane. The most significant features are an upper-bound $m_{\tilde{\chi}_1^0} \lesssim 500$ GeV, required to satisfy $(g-2)_\mu$, a lower-bound on the chargino co-annihilation region at $m_{\tilde{\chi}_1^0} \simeq 103$ GeV from LEP limits and the light-Higgs- and Z-funnel regions at $m_{\tilde{\chi}_1^0} \simeq 62$ GeV and $m_{\tilde{\chi}_1^0} \simeq 45$ GeV respectively.

In the pMSSM11 scenario, an extended study of the impact of LHC run-2 constraints and of $(g-2)_\mu$ on the allowed parameter space has been performed [47]. Moreover, for the first time LHC run-2 constraints on electroweakinos have been included, still using a `FastLim`-like approach and a recently developed tool, `EWKFast` [92], which allows the fast computation of electroweakino production cross-sections at NLO-QCD. The one additional free parameter

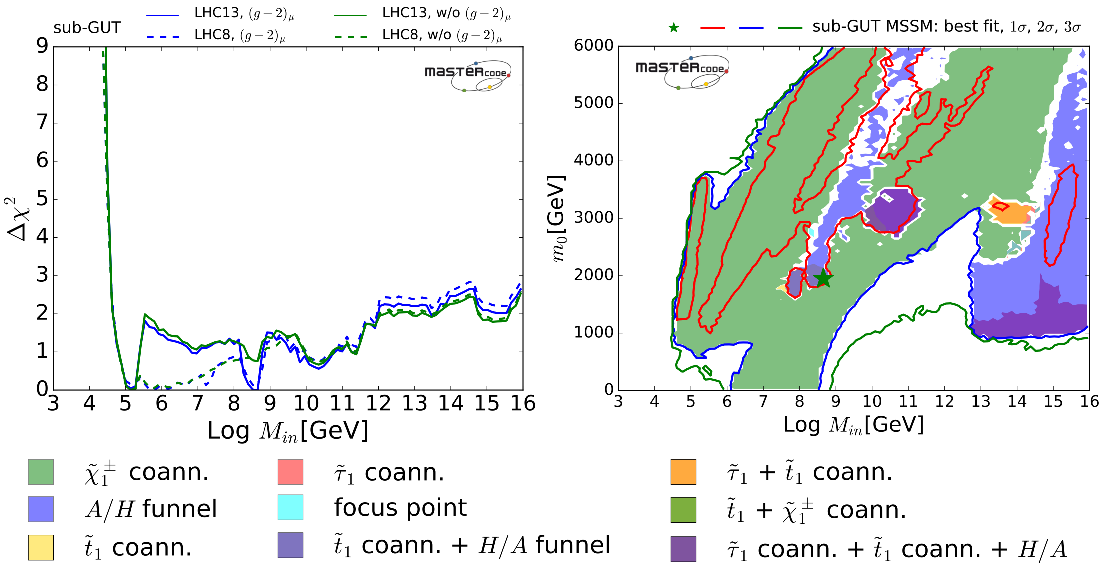

Figure 10: On the left, we show the one-dimensional likelihood profiles for the input scale $M_{\rm in}$ of the soft SUSY-breaking terms. We show four different profiles, with (solid) and without (dashed) the constraints coming from the direct searches for coloured superpartners and heavy Higgses at LHC run-2 and with (blue) and without (green) the constraint coming from the $(g-2)_\mu$ anomaly. On the right, we display the two-dimensional likelihood profiles at 68%/95%/99% CL in the $\log(M_{\rm in})$-m_0 plane, with the full constraint set applied. The colour shadings indicate the dominant mechanism which moves the CDM density into the allowed range from cosmological observations. Figures taken from Ref. [91].

with respect to the pMSSM10 (the soft SUSY-breaking mass terms for the $\tilde{\tau}$) changed the phenomenology by introducing a new relic density mechanism, slepton co-annihilation.

Fig. 12 (left) shows again the one-dimensional likelihood profile for the SUSY contribution to $(g-2)_\mu$, with and without the constraints from searches of SUSY particles at the LHC at 13 TeV and with and without imposing the $(g-2)_\mu$ constraint. In the pMSSM11 the displayed range of values can be covered, including the region consistent with the experimental measurement. Fig. 12 (right) shows the $m_{\tilde{\chi}_1^0}$-σ_p^{SI} plane *without* imposing the $(g-2)_\mu$ constraint. The best fit region moves to larger masses, where the neutralino has a mas of $\simeq 1$ TeV and it is Higgsino-like. This change in the location of the preferred region is a result of an improved compatibility with the flavour constraints, especially $\mathrm{BR}(B_{s,d} \to \mu^\pm\mu^\mp)$.

Since phenomenological scenarios such as the pMSSM11 have more room for light SUSY spectra, it is interesting to study the impact of the LHC run-2 results and the most recent direct detection experiments. Fig. 13 (left) shows the change in $m_{\tilde{q}_{1,2}}$-$m_{\tilde{g}}$ plane after including the aforementioned results. The shift from LHC searches performed at 8 TeV to the ones at the 13 TeV produces a marked change in the likelihood contours, shifting the lowest allowed mass for the first two-generation squarks and the gluino by a sizable amount, excluding completely the compressed region at low squark-/gluino-mass which was allowed by the LHC run-1 results and shifting the boundaries of the non-compressed region by $\simeq$ 500-1000 GeV. Fig. 13 (right)

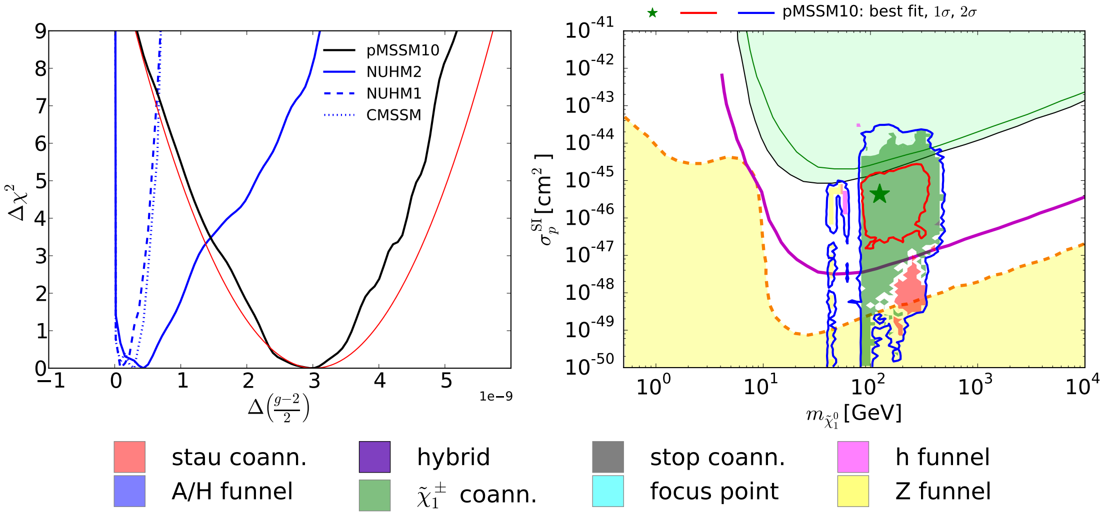

Figure 11: On the left, the one-dimensional likelihood profile for the SUSY contribution to $\Delta((g-2)/2)$ in the pMSSM10 and the CMSSM, NUHM1 and NUHM2. On the right, the two-dimensional likelihood profiles in the pMSSM10 in the $m_{\tilde{\chi}^0_1}$-σ_p^{SI} plane. The colour shadings indicate the dominant mechanism which moves the CDM density into the allowed range from cosmological observations. Figures taken from Refs. [46] and [86], respectively.

shows the same result without using the $(g-2)_\mu$ constraint. Lower masses are allowed in this case since larger neutralino masses are allowed and more compressed spectra are possible which evade the LHC bounds.

5 Fits of other BSM models

5.1 Oblique parameters from the global electroweak fit

New physics effects from virtual particles in loops can contribute through vacuum polarization corrections to the electroweak precision observables if the scale of new physics is larger than the electroweak scale. These effects are conveniently parametrised by the three self-energy parameters S, T, and U [93,94] describing the difference between the oblique vacuum corrections as determined from the experimental data and the corrections expected in a reference SM (with fixed reference values of m_t and M_H). The parameters S and T describe new physics contributions to neutral weak currents and to the difference between neutral and charged weak current processes, respectively. The U parameter is only constrained by the W boson mass and width, it is predicted to be small in most new physics models and often set to zero. The S, T, and U parameters are normalised such that the expected BSM contributions are of order $\mathcal{O}(1)$. The global electroweak fit can be used to determine S, T and U. Significant deviation of the results from zero are an unambiguous hint for new physics.

For reference values of $M_{H,\mathrm{ref}} = 125\,\mathrm{GeV}$ and $m_{t,\mathrm{ref}} = 172.5\,\mathrm{GeV}$ the following values are obtained [11] using the `Gfitter` framework: $S = 0.04 \pm 0.11$, $T = 0.09 \pm 0.14$, $U = -0.02 \pm 0.11$ with correlation coefficients of $+0.92$ between S and T, -0.68 between S and

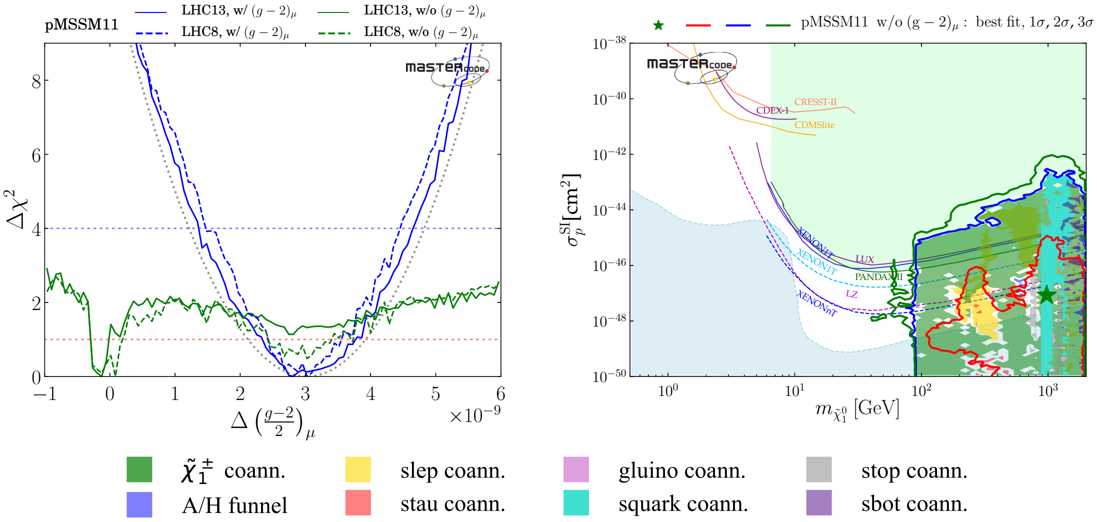

Figure 12: On the left, the one-dimensional likelihood profile for the SUSY contribution to $\Delta((g-2)/2)$ in the pMSSM11. We show four different profiles, with (solid) and without (dashed) the constraints coming from the direct searches for coloured superpartners at LHC run-2 and with (blue) and without (green) the constraint coming from $(g-2)_\mu$. On the right, the two-dimensional likelihood profiles in the pMSSM11 in the $m_{\tilde{\chi}_1^0}$-σ_p^{SI} plane. The colour shadings indicate the dominant mechanism which moves the CDM density into the allowed range from cosmological observations. Figures taken from Ref. [47].

U and -0.87 between T and U. The 68 % and 95 % CL allowed regions on S and T for a fixed value of $U = 0$ are shown in Fig.14. The constraints obtained for individual observables with strongest sensitivities are compatible with each other and their combination yields allowed regions in agreement with the prediction of the reference SM. These results on the oblique parameters are used by analyses to constrain the allowed parameter regions of new physics models. Example results for such analyses before the Higgs boson discovery are derived in [8] for a fourth fermion generation, two Higgs doublet, inert Higgs and littlest Higgs models, models with large, universal or warped extra dimensions and technicolour.

5.2 Global fits of two-Higgs-doublet models

A popular extension of the minimal Higgs sector, as implemented in the SM, are Two-Higgs-doublet models (2HDM) [95] which only introduce an additional $SU(2)_L \times U(1)_Y$ Higgs doublet field with hypercharge $Y = 1$, leading to five physical Higgs bosons h, H, A, H^+, and H^-. The neutral h can be identified with the 125 GeV Higgs boson as discovered at the LHC. Free model parameters of the 2HDM are the masses of these boson states M_{A^0}, M_{h^0}, M_{H^0} and $M_{H^\pm}$, the ratio of the vacuum expectation values of the two Higgs doublets $\tan\beta = v_2/v_1$ and the angle α describing the mixing of the two neutral Higgs fields h and H. In general, the 2HDM may lead to flavour-changing neutral currents (FCNCs) and CP violating interactions which can be avoided by fixing the Higgs boson couplings for up-type quarks, down-type quarks and leptons to specific values [95, 96]. Most popular CP conserving 2HDM scenarios include the *Type-I*

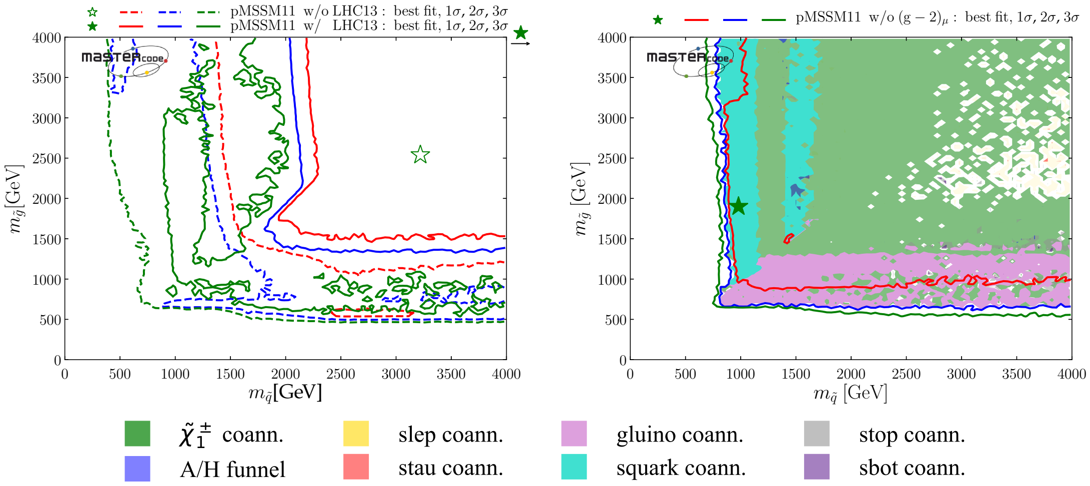

Figure 13: On the left, we show the two-dimensional likelihood profiles in the $m_{\tilde{q}_{1,2}}$-$m_{\tilde{g}}$ plane before (dashed lines) and after (solid lines) applying the constraints coming from LHC run-2 results, including flavour, and from the results of direct detection experiments after 2015. On the right, we display the same plane, with the full constraint set applied but for $(g-2)_\mu$. The colour shadings represent the dominant DM mechanism, with the colour coding defined in the legend below the plots. Figures taken from Ref. [47].

scenario, the *Type-II* scenario, the *lepton specific* scenario, and the *flipped* scenario.

Measurements of observables with sensitivity to the existence of the additional 2HDM Higgs bosons via quantum corrections can be used in global fits to constrain the allowed ranges of the Higgs boson masses and mixing angles in these scenarios. Within this project we performed several 2HDM analyses using the `Gfitter` framework. A first analysis before the Higgs discovery [7] was restricted to the Type-II scenario and only included observables sensitive to corrections from the exchange of a charged Higgs boson. At the time, the most stringent constraints have been obtained from rare radiative and leptonic decays of B and K mesons in which the charged Higgs boson replaces a SM W boson in the charged current process. A second 2HDM analysis [8] showed that constraints from the oblique parameters (cf. Sec. 5.1) do not allow a determination of any of the free 2HDM parameters independently of the values of the other parameters. A third analysis [11] after the Higgs boson discovery used individually the data from Higgs boson coupling measurements, from flavour observables (mainly branching fractions of B, D and K mesons), the anomalous magnetic moment of the muon, and the electroweak precision data via the oblique parameters and combined them in a global fit. In the following only results of this most recent study are discussed.

By construction of the four 2HDM scenarios considered, FCNC transitions are forbidden at tree-level and flavour violation can only arise at loop level by the exchange of a charged Higgs boson with strength depending on $M_{H^\pm}$ and $\tan\beta$. Example constraints obtained from the individual flavour observables are shown in Fig. 15 (left) where the excluded parameter regions (95 % CL) in the Type-II scenario are shown in the plane of these two sensitive parameters. Most stringent constraints are obtained from the branching fraction $\mathcal{B}(b \to X_s\gamma)$ which allows to exclude $M_{H^\pm} < 590\,\text{GeV}$. It is interesting to note that the measurements of the semileptonic

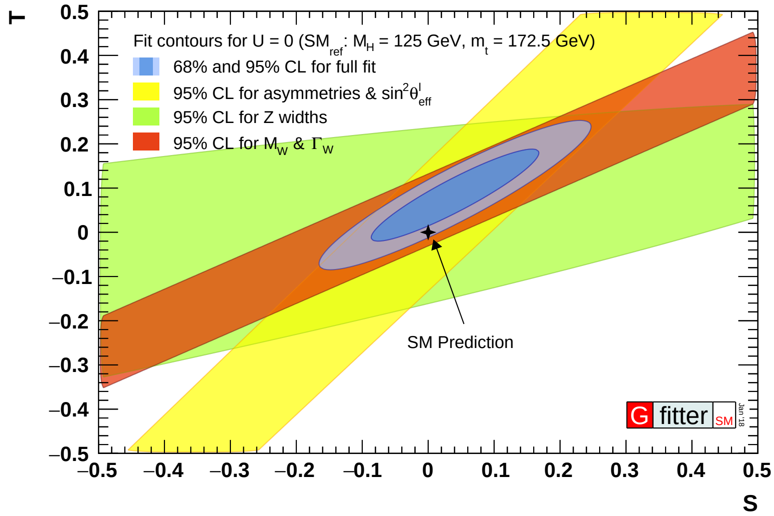

Figure 14: Allowed regions of the oblique parameters S and T, with the U parameter fixed to zero, as obtained from the global electroweak fit using all observables (blue) and for individual sensitive observables (yellow, green, red). Figure taken from Ref. [11].

decay ratios of neutral B mesons $R(D)$ and $R(D^*)$ which differ from their SM predictions [97] only feature a compatible parameter region in the Type-II scenario which is however excluded by several other observables (not shown in the figure).

Example constraints for the Type-II scenario from the combined analysis of Higgs coupling measurements, flavour observables, magnetic moment of the muon and the oblique parameters are shown in Fig. 15 (right) where the resulting 68 % and 95 % CL allowed regions in the M_A versus M_H plane are shown for a fixed charged Higgs boson mass of 750 GeV. All other 2HDM parameters are allowed to vary freely. A strong alignment of either the H or the A boson mass with the mass of the $H^\pm$ can be observed (this is true for all 2HDM scenarios considered) as a result of constraints on $\beta - \alpha$ obtained from the Higgs coupling strength measurements. For the Type-II scenario (and the flipped scenario, not shown) pairs of (H, A) masses below $\sim$ 400 GeV are excluded as indicated by the hatched regions where also results of different statistical interpretations are illustrated by red and green lines. However, our analysis also demonstrated that no absolute mass limits can be derived with current data for the Type-I and lepton specific scenarios.

5.3 Constraints on Higgs physics-relevant $d = 6$ operators

If new physical effects stay elusive and direct searches for new physics at the LHC continue to produce null results, this could point towards high-scale new physics. While no new states would be observable at energy scales reachable at the LHC, this nevertheless can lead to subtle deviations from SM expectations which might still be observable. In this scenario, not a single measurement alone would lead to a discovery, but small hints would emerge in a number of different channels.

Under this predicament, the most promising avenue for finding new physics are precision

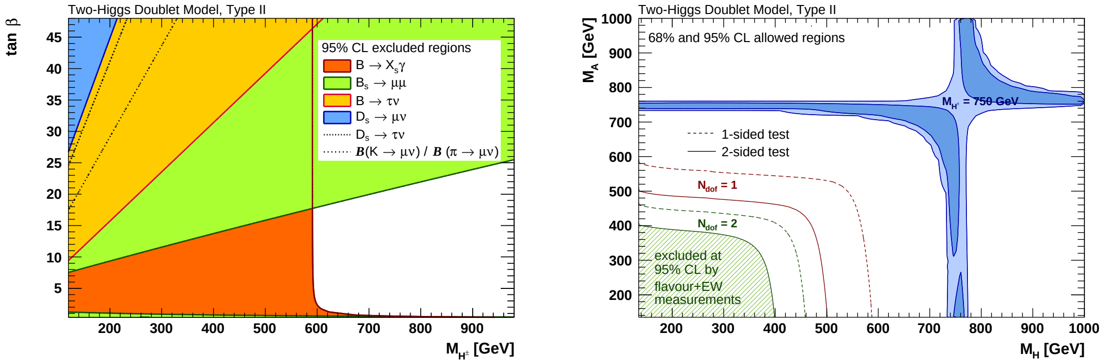

Figure 15: Results of fits of 2HDM models of Type II: (left) excluded parameter regions in the $\tan\beta$ versus $M_{H^\pm}$ plane as obtained from individual flavour observables; (right) allowed regions in the M_A versus M_H plane as obtained from a combined fit of constraints from the Higgs boson coupling strength measurements, flavour observables, muon anomalous magnetic moment and electroweak precision data. Figures taken from Ref. [11].

studies of Higgs production, which is the least constraint sector of the SM. This motivates the extension of the Lagrangian of the Higgs sector by dimension six ($d = 6$) operators

$$\mathcal{L}_{\text{Higgs}} = \mathcal{L}_{\text{Higgs}}^{\text{SM}} + \sum_i \frac{c_i}{\Lambda^2} O_i \tag{1}$$

to capture new interactions beyond the Standard Model (BSM) in a model-independent way. The first term on the right-hand side of Eq. 1 is the SM Lagrangian of the Higgs sector, while the second term denotes BSM contributions from $d = 6$ operators O_i, which scale with the Wilson coefficients c_i over the square of the scale of new physics Λ^2. This extension assumes that all unknown states have been integrated out and only the effect of the resulting $d = 6$ operators are observable at present colliders. An important question that arises is the extent to which it will be possible to probe the presence of such interactions. Or equivalently, what are realistic estimates of Wilson coefficient constraints that can be expected after LHC run-2 and LHC run-3 or after the high luminosity phase of the LHC (HL-LHC) if direct hints for new physics will remain elusive?

To study this question the set of operators known as the strongly interacting light Higgs (SILH) Lagrangian in bar convention [98] has been considered in global analyses using the `Gfitter` framework [12, 13]. Focusing on the Higgs sector with flavour-diagonal dimension six effects and respecting constraints from oblique corrections to LEP data through the S and T parameters, the number of relevant operators is eight. Using LHC run-1 Higgs data from ATLAS and CMS two coefficients, $\bar{c}_g$ and $\bar{c}_\gamma$, can be reliably constrained in a global fit at 95% CL:

$$\begin{aligned} \bar{c}_g &\in [\,-0.64,\, 0.43\,] \times 10^{-4} \\ \bar{c}_\gamma &\in [\,-7.8,\, 4.3\,] \times 10^{-4}\,, \end{aligned} \tag{2}$$

where the constraints from the likelihood scan of $\bar{c}_g$ are shown in Fig. 16 (left). There are no noteworthy constraints on the other six operators from LHC run-1 data, which is only partially

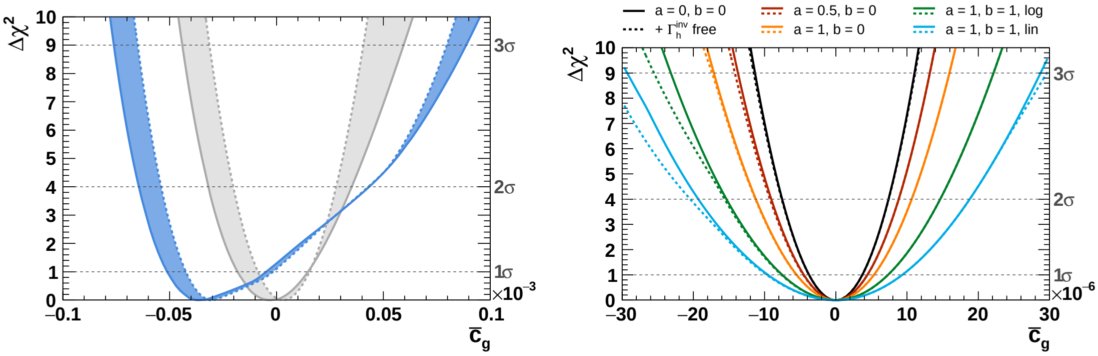

Figure 16: Constraints of the Wilson coefficient $\bar{c}_g$: results as obtained from the LHC run-1 data-set (left). The solid (dashed) line corresponds to a fit with theoretical uncertainties included (excluded). The grey band denotes the individual constraints on $\bar{c}_g$, and blue refers to the marginalised result; sensitivity projection for HL-LHC using differential Higgs p_T distributions (right). Figures taken from Refs. [12] and [13], respectively.

due to the insufficient precision of these data. When projecting to the expected precision achieved after the HL-LHC, still a number of operators cannot be constrained in a global fit [12] due to so-called flat directions in the multi-dimensional parameter space, which are due to effects from new physics that cancel out on inclusive Higgs observables and hence lead to unobservable BSM contributions.

These flat directions can be lifted by including measurements of differential distributions of Higgs boson production, most notably the Higgs boson transverse momentum p_T. The reason for this is the large effect of BSM contributions to the tails of the p_T distributions. When including measurements in all observable Higgs production modes and decay channels at the LHC, the effects of the various $d = 6$ operators do not cancel out fully anymore leading to the prospect of constraints on all operators, albeit the constraints on the Higgs-fermion operators will stay weaker than the ones on the Higgs boson ones. The likelihood scans shown in Fig. 16 (right) show the constraints on $\bar{c}_g$ obtained from pseudo data extrapolated to the HL-LHC precision. The different colours denote assumptions on the theoretical uncertainties, and dashed lines have been obtained in a scenario where an additional unobservable contribution to the total width of the Higgs boson from light degrees of freedom has been taken into account. While there are differences of up to a factor of two on the sensitivity at 95% CL for different assumptions, even with overly pessimistic theoretical uncertainties in the tails of the distributions ($a = 1$, $b = 1$, lin), stronger bounds can be obtained than by considering signal strength measurements only [13]. In this sense, differential measurements of Higgs boson production can help to improve the physics potential of the LHC when combined in a global fit with inclusive data.

6 Conclusions

We have summarized the highlight results of the project B8 of the SFB 676: developments of the software tools `Gfitter`, `Fittino`, `MasterCode`, `HiggsBounds` and `HiggsSignals` as well as physics results obtained from the application of these tools in global fits of the SM, supersymmetric models and further extensions of the SM.

The experimental results used in the global fits consist of measurements of electroweak precision observables, measurements of the properties of the Higgs signal at 125 GeV, limits from searches for additional Higgs bosons and further states of physics scenarios beyond the SM, results from flavor physics, the dark matter relic density and further astrophysical data. If the results of the dark matter relic density and the magnetic moment of the muon are discarded from the considered data set, the SM with a Higgs boson at 125 GeV is compatible with the experimental results at the present level. However, the same is true, even after including the dark matter relic density and the magnetic moment of the muon, for various supersymmetric extensions of the SM and further scenarios of new physics. We have determined the parameter regions that are preferred by the current data, for a variety of models, which represent attractive alternatives to the SM and are based on fundamentally different physics assumptions.

The identification of the mechanism of electroweak symmetry breaking and more generally the structure of the electroweak and strong interactions will continue to be a prime target of particle physics research during the next decades. The prospective improvements in experimental precision in combination with corresponding efforts in theoretical calculations will significantly enhance the sensitivity for discriminating between different realisations of the underlying dynamics, and global fits will be of crucial importance for accomplishing this task. The results of this project constitute a significant progress in this area and provide the foundations for future analyses.

Acknowledgements

E. B. and G. W. would like to thank their collaborators on the `MasterCode` project, J.C. Costa, M. Borsato, O. Buchmueller, R. Cavanaugh, M. Citron, A. De Roeck, M.J. Dolan, J.R. Ellis, H. Flächer, S. Heinemeyer, G. Isidori, M. Lucio, D. Martínez Santos, K.A. Olive, A. Richards, K. Sakurai and K.J. De Vries. J. H., R. K. and T. P. would like to thank the current and past members of the `Gfitter` group for their collaboration and support, M. Baak, J. Cuth, H. Flächer, M. Goebel, A. Hoecker, D. Kennedy, K. Mönig, M. Schott and J. Stelzer. P. B. and T. S. would like to thank the current and past members of the `Fittino` group, K. Desch, H. Dreiner, M. Hamer, M. Krämer, B. O'Leary, W. Porod, B. Sarrazin, M. Uhlenbrock and P. Wienemann. P. B., T. S. and G. W. would like to thank the current and past members of the `HiggsBounds` and `HiggsSignals` projects for their collaboration and support, O. Brein, S. Heinemeyer, O. Stål, K.E. Williams. We would furthermore like to thank H. Haber, A. Weiler and L. Zeune for fruitful collaboration.
The work presented in this report has been supported in part by the DFG through the SFB 676 "Particles, Strings and the Early Universe".

References

[1] SLD Electroweak Group, DELPHI, ALEPH, SLD, SLD Heavy Flavour Group, OPAL, LEP Electroweak Working Group, L3, S. Schael et al., *Precision electroweak measurements on the Z resonance*, *Phys. Rept.* **427** (2006) 257–454, [hep-ex/0509008].

[2] The yearly reports of the LEP Electroweak Working Group can be found at http://lepewwg.web.cern.ch/LEPEWWG/stanmod.

[3] All versions of the PDG particle listings and reviews can be found at http://pdg.lbl.gov/2016/html/rpp_archives.html.

[4] Gfitter Group. Results at http://cern.ch/gfitter.

[5] HEPfit Group. Results at http://hepfit.roma1.infn.it.

[6] M. Baak, J. Haller and K. Mönig, *Global Fits of the Electroweak Standard Theory: Past, Present and Future*, *Adv. Ser. Direct. High Energy Phys.* **26** (2016) 215–229.

[7] Gfitter Group, H. Flacher, M. Goebel, J. Haller, A. Hocker, K. Monig and J. Stelzer, *Revisiting the Global Electroweak Fit of the Standard Model and Beyond with Gfitter*, *Eur. Phys. J.* **C60** (2009) 543–583, [0811.0009]. [Erratum: *Eur. Phys. J.* **C71** (2011) 1718].

[8] Gfitter Group, M. Baak, M. Goebel, J. Haller, A. Hoecker, D. Ludwig, K. Moenig et al., *Updated Status of the Global Electroweak Fit and Constraints on New Physics*, *Eur. Phys. J.* **C72** (2012) 2003, [1107.0975].

[9] Gfitter Group, M. Baak, M. Goebel, J. Haller, A. Hoecker, D. Kennedy, R. Kogler et al., *The Electroweak Fit of the Standard Model after the Discovery of a New Boson at the LHC*, *Eur. Phys. J.* **C72** (2012) 2205, [1209.2716].

[10] Gfitter Group, M. Baak, J. Cúth, J. Haller, A. Hoecker, R. Kogler, K. Mönig et al., *The global electroweak fit at NNLO and prospects for the LHC and ILC*, *Eur. Phys. J.* **C74** (2014) 3046, [1407.3792].

[11] Gfitter Group, J. Haller, A. Hoecker, R. Kogler, K. Mönig, T. Peiffer and J. Stelzer, *Update of the global electroweak fit and constraints on two-Higgs-doublet models*, *Eur. Phys. J.* **C78** (2018) 675, [1803.01853].

[12] C. Englert, R. Kogler, H. Schulz and M. Spannowsky, *Higgs coupling measurements at the LHC*, *Eur. Phys. J.* **C76** (2016) 393, [1511.05170].

[13] C. Englert, R. Kogler, H. Schulz and M. Spannowsky, *Higgs characterisation in the presence of theoretical uncertainties and invisible decays*, *Eur. Phys. J.* **C77** (2017) 789, [1708.06355].

[14] D0 Collaboration, S. Abachi et al., *Observation of the top quark*, *Phys. Rev. Lett.* **74** (1995) 2632–2637, [hep-ex/9503003].

[15] CDF Collaboration, F. Abe et al., *Observation of top quark production in $\bar{p}p$ collisions*, *Phys. Rev. Lett.* **74** (1995) 2626–2631, [hep-ex/9503002].

[16] ATLAS Collaboration, G. Aad et al., *Observation of a new particle in the search for the Standard Model Higgs boson with the ATLAS detector at the LHC*, *Phys. Lett.* **B716** (2012) 1–29, [1207.7214].

[17] CMS Collaboration, S. Chatrchyan et al., *Observation of a new boson at a mass of 125 GeV with the CMS experiment at the LHC*, *Phys. Lett.* **B716** (2012) 30–61, [1207.7235].

[18] ATLAS, CMS Collaborations, G. Aad et al., *Combined Measurement of the Higgs Boson Mass in pp Collisions at $\sqrt{s} = 7$ and 8 TeV with the ATLAS and CMS Experiments*, *Phys. Rev. Lett.* **114** (2015) 191803, [1503.07589].

[19] Particle Data Group, C. Patrignani et al., *Review of Particle Physics*, *Chin. Phys.* **C40** (2016) 100001.

[20] DELPHI, OPAL, LEP Electroweak, ALEPH, L3 Collaborations, S. Schael et al., *Electroweak Measurements in Electron-Positron Collisions at W-Boson-Pair Energies at LEP*, *Phys. Rept.* **532** (2013) 119–244, [1302.3415].

[21] CDF, D0 Collaborations, T. E. W. Group, *2012 Update of the Combination of CDF and D0 Results for the Mass of the W Boson*, 1204.0042.

[22] ATLAS Collaboration, M. Aaboud et al., *Measurement of the W-boson mass in pp collisions at $\sqrt{s} = 7$ TeV with the ATLAS detector*, *Eur. Phys. J.* **C78** (2018) 110, [1701.07240].

[23] CDF, D0 Collaborations, T. A. Aaltonen et al., *Tevatron Run II combination of the effective leptonic electroweak mixing angle*, *Phys. Rev.* **D97** (2018) 112007, [1801.06283].

[24] M. Davier, A. Hoecker, B. Malaescu and Z. Zhang, *Reevaluation of the hadronic vacuum polarisation contributions to the Standard Model predictions of the muon $g-2$ and $\alpha(m_Z^2)$ using newest hadronic cross-section data*, *Eur. Phys. J.* **C77** (2017) 827, [1706.09436].

[25] OPAL, DELPHI, LEP Working Group for Higgs boson searches, ALEPH, L3, R. Barate et al., *Search for the standard model Higgs boson at LEP*, *Phys. Lett.* **B565** (2003) 61–75, [hep-ex/0306033].

[26] CDF, D0 Collaborations, T. T. E. V. N. P. H. W. Group, *Combined CDF and D0 Upper Limits on Standard Model Higgs-Boson Production with up to 6.7 fb^{-1} of Data*, in *Proceedings, 35th International Conference on High energy physics (ICHEP 2010): Paris, France, July 22-28, 2010*, 2010, 1007.4587.

[27] DELPHI, OPAL, ALEPH, LEP Working Group for Higgs Boson Searches, L3, S. Schael et al., *Search for neutral MSSM Higgs bosons at LEP*, *Eur. Phys. J.* **C47** (2006) 547–587, [hep-ex/0602042].

[28] D0 Collaboration, V. M. Abazov et al., *Search for Higgs bosons of the minimal supersymmetric standard model in $p\bar{p}$ collisions at $\sqrt(s) = 1.96$ TeV*, *Phys. Lett.* **B710** (2012) 569–577, [1112.5431].

[29] CDF Collaboration, T. Aaltonen et al., *Search for Higgs bosons predicted in two-Higgs-doublet models via decays to tau lepton pairs in 1.96-TeV p anti-p collisions*, *Phys. Rev. Lett.* **103** (2009) 201801, [0906.1014].

[30] P. Bechtle, O. Brein, S. Heinemeyer, G. Weiglein and K. E. Williams, *HiggsBounds: Confronting Arbitrary Higgs Sectors with Exclusion Bounds from LEP and the Tevatron*, *Comput. Phys. Commun.* **181** (2010) 138–167, [0811.4169].

[31] P. Bechtle, O. Brein, S. Heinemeyer, G. Weiglein and K. E. Williams, *HiggsBounds 2.0.0: Confronting Neutral and Charged Higgs Sector Predictions with Exclusion Bounds from LEP and the Tevatron*, *Comput. Phys. Commun.* **182** (2011) 2605–2631, [1102.1898].

[32] P. Bechtle, O. Brein, S. Heinemeyer, O. Stal, T. Stefaniak, G. Weiglein et al. code available from http://higgsbounds.hepforge.org/.

[33] P. Bechtle, O. Brein, S. Heinemeyer, O. Stål, T. Stefaniak, G. Weiglein et al., HiggsBounds − 4*: Improved Tests of Extended Higgs Sectors against Exclusion Bounds from LEP, the Tevatron and the LHC*, *Eur. Phys. J.* **C74** (2014) 2693, [1311.0055].

[34] P. Bechtle, S. Heinemeyer, O. Stal, T. Stefaniak and G. Weiglein, *Applying Exclusion Likelihoods from LHC Searches to Extended Higgs Sectors*, *Eur. Phys. J.* **C75** (2015) 421, [1507.06706].

[35] CMS Collaboration, V. Khachatryan et al., *Search for neutral MSSM Higgs bosons decaying to a pair of tau leptons in pp collisions*, *JHEP* **10** (2014) 160, [1408.3316].

[36] ATLAS, CMS Collaborations, G. Aad et al., *Measurements of the Higgs boson production and decay rates and constraints on its couplings from a combined ATLAS and CMS analysis of the LHC pp collision data at $\sqrt{s} = 7$ and 8 TeV*, *JHEP* **08** (2016) 045, [1606.02266].

[37] P. Bechtle, S. Heinemeyer, O. Stal, T. Stefaniak, G. Weiglein and L. Zeune, *MSSM Interpretations of the LHC Discovery: Light or Heavy Higgs?*, *Eur. Phys. J.* **C73** (2013) 2354, [1211.1955].

[38] P. Bechtle, S. Heinemeyer, O. Stål, T. Stefaniak and G. Weiglein, *HiggsSignals: Confronting arbitrary Higgs sectors with measurements at the Tevatron and the LHC*, *Eur. Phys. J.* **C74** (2014) 2711, [1305.1933].

[39] P. Bechtle, S. Heinemeyer, O. Stål, T. Stefaniak and G. Weiglein, *Probing the Standard Model with Higgs signal rates from the Tevatron, the LHC and a future ILC*, *JHEP* **11** (2014) 039, [1403.1582].

[40] LHC Higgs Cross Section Working Group, D. de Florian et al., *Handbook of LHC Higgs Cross Sections: 4. Deciphering the Nature of the Higgs Sector*, 1610.07922.

[41] P. Bechtle, H. E. Haber, S. Heinemeyer, O. Stål, T. Stefaniak, G. Weiglein et al., *The Light and Heavy Higgs Interpretation of the MSSM*, *Eur. Phys. J.* **C77** (2017) 67, [1608.00638].

[42] F. Domingo and G. Weiglein, *NMSSM interpretations of the observed Higgs signal*, *JHEP* **04** (2016) 095, [1509.07283].

[43] P. Drechsel, L. Galeta, S. Heinemeyer and G. Weiglein, *Precise Predictions for the Higgs-Boson Masses in the NMSSM*, *Eur. Phys. J.* **C77** (2017) 42, [1601.08100].

[44] Planck Collaboration, P. A. R. Ade et al., *Planck 2013 results. XVI. Cosmological parameters*, *Astron. Astrophys.* **571** (2014) A16, [1303.5076].

[45] Muon G-2 Collaboration, G. Bennett et al., *Final Report of the Muon E821 Anomalous Magnetic Moment Measurement at BNL*, *Phys.Rev.* **D73** (2006) 072003, [hep-ex/0602035].

[46] K. J. de Vries et al., *The pMSSM10 after LHC Run 1*, *Eur. Phys. J.* **C75** (2015) 422, [1504.03260].

[47] E. Bagnaschi et al., *Likelihood Analysis of the pMSSM11 in Light of LHC 13-TeV Data*, *Eur. Phys. J.* **C78** (2018) 256, [1710.11091].

[48] O. Buchmueller et al., *The CMSSM and NUHM1 after LHC Run 1*, *Eur. Phys. J.* **C74** (2014) 2922, [1312.5250].

[49] O. Buchmueller et al., *The NUHM2 after LHC Run 1*, *Eur. Phys. J.* **C74** (2014) 3212, [1408.4060].

[50] M. Cannoni, J. Ellis, M. E. Gómez, S. Lola and R. Ruiz de Austri, *Supersymmetry Searches in GUT Models with Non-Universal Scalar Masses*, *JCAP* **1603** (2016) 041, [1511.06205].

[51] E. Bagnaschi et al., *Likelihood Analysis of the Minimal AMSB Model*, *Eur. Phys. J.* **C77** (2017) 268, [1612.05210].

[52] P. Bechtle, K. Desch and P. Wienemann, *Fittino, a program for determining MSSM parameters from collider observables using an iterative method*, *Comput. Phys. Commun.* **174** (2006) 47–70, [hep-ph/0412012].

[53] P. Bechtle et al., *Killing the cMSSM softly*, *Eur. Phys. J.* **C76** (2016) 96, [1508.05951].

[54] P. Bechtle, K. Desch, M. Uhlenbrock and P. Wienemann, *Constraining SUSY models with Fittino using measurements before, with and beyond the LHC*, *Eur. Phys. J.* **C66** (2010) 215–259, [0907.2589].

[55] P. Bechtle, B. Sarrazin, K. Desch, H. K. Dreiner, P. Wienemann, M. Kramer et al., *What if the LHC does not find supersymmetry in the* $\sqrt{s} = 7$ *TeV run?*, *Phys. Rev.* **D84** (2011) 011701, [1102.4693].

[56] P. Bechtle et al., *Constrained Supersymmetry after two years of LHC data: a global view with Fittino*, *JHEP* **06** (2012) 098, [1204.4199].

[57] M. Kramer et al., *Constrained supersymmetric models in the light of LHC exclusions, precision measurements and astroparticle physics*, *Frascati Phys. Ser.* **54** (2012) 258–266.

[58] A. De Roeck et al., *From the LHC to Future Colliders*, *Eur. Phys. J.* **C66** (2010) 525–583, [0909.3240].

[59] GAMBIT Collaboration, G. D. Martinez, J. McKay, B. Farmer, P. Scott, E. Roebber, A. Putze et al., *Comparison of statistical sampling methods with ScannerBit, the GAMBIT scanning module*, *Eur. Phys. J.* **C77** (2017) 761, [1705.07959].

[60] W. Porod and F. Staub, *SPheno 3.1: Extensions including flavour, CP-phases and models beyond the MSSM*, *Comput.Phys.Commun.* **183** (2012) 2458–2469, [1104.1573].

[61] F. Mahmoudi, *SuperIso v2.3: A Program for calculating flavor physics observables in Supersymmetry*, *Comput.Phys.Commun.* **180** (2009) 1579–1613, [0808.3144].

[62] G. Belanger, F. Boudjema, A. Pukhov and A. Semenov, *MicrOMEGAs: A Program for calculating the relic density in the MSSM*, *Comput.Phys.Commun.* **149** (2002) 103–120, [hep-ph/0112278].

[63] S. Heinemeyer, W. Hollik and G. Weiglein, *FeynHiggs: A Program for the calculation of the masses of the neutral CP even Higgs bosons in the MSSM*, *Comput. Phys. Commun.* **124** (2000) 76–89, [hep-ph/9812320].

[64] P. Bechtle, S. Belkner, D. Dercks, M. Hamer, T. Keller, M. Krämer et al., *SCYNet: Testing supersymmetric models at the LHC with neural networks*, *Eur. Phys. J.* **C77** (2017) 707, [1703.01309].

[65] M. Drees, H. Dreiner, D. Schmeier, J. Tattersall and J. S. Kim, *CheckMATE: Confronting your Favourite New Physics Model with LHC Data*, *Comput. Phys. Commun.* **187** (2015) 227–265, [1312.2591].

[66] J. Albrecht, F. Bernlochner, M. Kenzie, S. Reichert, D. Straub and A. Tully, *Future prospects for exploring present day anomalies in flavour physics measurements with Belle II and LHCb*, 1709.10308.

[67] P. Z. Skands et al., *SUSY Les Houches accord: Interfacing SUSY spectrum calculators, decay packages, and event generators*, *JHEP* **07** (2004) 036, [hep-ph/0311123].

[68] T. Hahn, *SUSY Les Houches Accord 2 I/O made easy*, *Comput. Phys. Commun.* **180** (2009) 1681–1693, [hep-ph/0605049].

[69] B. C. Allanach, *SOFTSUSY: a program for calculating supersymmetric spectra*, *Comput. Phys. Commun.* **143** (2002) 305–331, [hep-ph/0104145].

[70] S. Heinemeyer, W. Hollik and G. Weiglein, *The Masses of the neutral CP - even Higgs bosons in the MSSM: Accurate analysis at the two loop level*, *Eur. Phys. J.* **C9** (1999) 343–366, [hep-ph/9812472].

[71] G. Degrassi, S. Heinemeyer, W. Hollik, P. Slavich and G. Weiglein, *Towards high precision predictions for the MSSM Higgs sector*, *Eur. Phys. J.* **C28** (2003) 133–143, [hep-ph/0212020].

[72] M. Frank et al., *The Higgs Boson Masses and Mixings of the Complex MSSM in the Feynman-Diagrammatic Approach*, *JHEP* **02** (2007) 047, [hep-ph/0611326].

[73] T. Hahn et al., *High-Precision Predictions for the Light CP -Even Higgs Boson Mass of the Minimal Supersymmetric Standard Model*, *Phys. Rev. Lett.* **112** (2014) 141801, [1312.4937].

[74] G. Belanger, F. Boudjema, A. Pukhov and A. Semenov, *micrOMEGAs_3: A program for calculating dark matter observables*, *Comput. Phys. Commun.* **185** (2014) 960–985, [1305.0237].

[75] G. Isidori and P. Paradisi, *Hints of large tan(beta) in flavour physics*, *Phys. Lett.* **B639** (2006) 499–507, [hep-ph/0605012].

[76] G. Isidori, F. Mescia, P. Paradisi and D. Temes, *Flavour physics at large tan(beta) with a Bino-like LSP*, *Phys. Rev.* **D75** (2007) 115019, [hep-ph/0703035].

[77] F. Mahmoudi, *SuperIso: A Program for calculating the isospin asymmetry of B —> K* gamma in the MSSM*, *Comput. Phys. Commun.* **178** (2008) 745–754, [0710.2067].

[78] D. Eriksson, F. Mahmoudi and O. Stal, *Charged Higgs bosons in Minimal Supersymmetry: Updated constraints and experimental prospects*, *JHEP* **11** (2008) 035, [0808.3551].

[79] S. Heinemeyer, W. Hollik, D. Stockinger, A. M. Weber and G. Weiglein, *Precise prediction for M(W) in the MSSM*, *JHEP* **08** (2006) 052, [hep-ph/0604147].

[80] S. Heinemeyer, W. Hollik, A. M. Weber and G. Weiglein, *Z Pole Observables in the MSSM*, *JHEP* **04** (2008) 039, [0710.2972].

[81] S. Heinemeyer, W. Hollik, G. Weiglein and L. Zeune, *Implications of LHC search results on the W boson mass prediction in the MSSM*, *JHEP* **12** (2013) 084, [1311.1663].

[82] F. Feroz and M. P. Hobson, *Multimodal nested sampling: an efficient and robust alternative to MCMC methods for astronomical data analysis*, *Mon. Not. Roy. Astron. Soc.* **384** (2008) 449, [0704.3704].

[83] F. Feroz, M. P. Hobson and M. Bridges, *MultiNest: an efficient and robust Bayesian inference tool for cosmology and particle physics*, *Mon. Not. Roy. Astron. Soc.* **398** (2009) 1601–1614, [0809.3437].

[84] F. Feroz, M. P. Hobson, E. Cameron and A. N. Pettitt, *Importance Nested Sampling and the MultiNest Algorithm*, 1306.2144.

[85] J. Gomes, I. Campos, E. Bagnaschi, M. David, L. Alves, J. Martins et al., *Enabling rootless Linux Containers in multi-user environments: the udocker tool*, *Comput. Phys. Commun.* **232** (2018) 84–97, [1711.01758].

[86] E. A. Bagnaschi et al., *Supersymmetric Dark Matter after LHC Run 1*, *Eur. Phys. J.* **C75** (2015) 500, [1508.01173].

[87] E. Bagnaschi et al., *Likelihood Analysis of Supersymmetric SU(5) GUTs*, *Eur. Phys. J.* **C77** (2017) 104, [1610.10084].

[88] M. Papucci, K. Sakurai, A. Weiler and L. Zeune, *Fastlim: a fast LHC limit calculator*, *Eur. Phys. J.* **C74** (2014) 3163, [1402.0492].

[89] W. Beenakker, M. Kramer, T. Plehn, M. Spira and P. M. Zerwas, *Stop production at hadron colliders*, *Nucl. Phys.* **B515** (1998) 3–14, [hep-ph/9710451].

[90] W. Beenakker, C. Borschensky, M. Krämer, A. Kulesza, E. Laenen, S. Marzani et al., *NLO+NLL squark and gluino production cross-sections with threshold-improved parton distributions*, *Eur. Phys. J.* **C76** (2016) 53, [1510.00375].

[91] J. C. Costa et al., *Likelihood Analysis of the Sub-GUT MSSM in Light of LHC 13-TeV Data*, *Eur. Phys. J.* **C78** (2018) 158, [1711.00458].

[92] E. Bagnaschi, P. Michele, K. Sakurai, W. A. and L. Zeune, *EWKFast: a fast calculator for EWKino production processes at the LHC*, *In preparation*, (2018) .

[93] M. E. Peskin and T. Takeuchi, *A New constraint on a strongly interacting Higgs sector*, *Phys. Rev. Lett.* **65** (1990) 964–967.

[94] M. E. Peskin and T. Takeuchi, *Estimation of oblique electroweak corrections*, *Phys. Rev.* **D46** (1992) 381–409.

[95] H. E. Haber, G. L. Kane and T. Sterling, *The Fermion Mass Scale and Possible Effects of Higgs Bosons on Experimental Observables*, *Nucl. Phys.* **B161** (1979) 493–532.

[96] G. C. Branco, P. M. Ferreira, L. Lavoura, M. N. Rebelo, M. Sher and J. P. Silva, *Theory and phenomenology of two-Higgs-doublet models*, *Phys. Rept.* **516** (2012) 1–102, [1106.0034].

[97] HFLAV Collaboration, Y. Amhis et al., *Averages of b-hadron, c-hadron, and τ-lepton properties as of summer 2016*, *Eur. Phys. J.* **C77** (2017) 895, [1612.07233].

[98] G. F. Giudice, C. Grojean, A. Pomarol and R. Rattazzi, *The Strongly-Interacting Light Higgs*, *JHEP* **06** (2007) 045, [hep-ph/0703164].